A novel subset of hepatocytes is simultaneously gluconeogenic and *de novo* lipogenic in the fed state and is naturally insulin resistant

Junichi Okada[1], Austin Landgraf[2], Maxwell Horton[2,3], Yunping Qiu[1,4], Alus M. Xiaoli[1,5], Roberto Ribas[6], Li Liu[1], Sofia V. Krylova[2], Victor L. Schuster[7], Fajun Yang[1,5], Takeshi Saito[8], Ramon C. Sun[6,9,10], Meredith Hawkins[1], Gary J Schwartz[1,11,12], Carolina Eliscovich[5,13], Kosaku Shinoda[1,2], Irwin J. Kurland[1,4] and Jeffrey E. Pessin[1,2]

[1]Departments of Medicine (Division of Endocrinology), [2]Molecular Pharmacology, [3]Biochemistry, [5]Developmental and Molecular Biology, [7]Medicine (Division of Nephrology), [11]Neuroscience, [12]Psychiatry and Behavioral Sciences and [13]Medicine (Hepatology). [4]Stable Isotope and Metabolomics Core Facility, New York Regional Diabetes Research Center. Fleischer Institute for Diabetes and Metabolism, The Albert Einstein College of Medicine, Bronx, NY 10461

[6]Department of Biochemistry and Molecular Biology, College of Medicine, University of Florida, Gainesville, FL 32610

[8]Department of Medicine, Division of Gastrointestinal and Liver Diseases, Immunology & Immune Therapeutics, and Pathology, Keck School of Medicine, University of Southern California, Los Angeles, CA 90033

[9]Center for Advanced Spatial Biomolecule Research, University of Florida, Gainesville, FL 32610

[10]Evelyn F. and William L. McKnight Brain Institute, University of Florida, Gainesville, FL 32610

Please address correspondences to:

Junichi Okada
Department of Medicine (Division of Endocrinology)
The Albert Einstein College of Medicine
369 Price Center, 1301 Morris Park Avenue
Bronx, NY 10461
Email: junichi.okada@einsteinmed.edu

ABSTRACT

It is generally accepted that hepatic gluconeogenesis, the synthesis of glucose from non-carbohydrate substrates is active in the fasted state and inactive in the fed state. In contrast, *de novo* lipogenesis is active in the fed state and is inactive in the fasted state. Here, we used targeted single cell RNA-seq, HCR RNA-FISH, and PrimeFlow in normal physiological mouse liver, and identified a subpopulation of periportal hepatocytes that simultaneously co-express both gluconeogenic and lipogenic genes in the fed state. Euglycemic-hyperinsulinemic clamps further demonstrated that this novel hepatocyte subpopulation is naturally insulin resistant. Spatial metabolic imaging coupled with stable isotope tracing analyses revealed individual hepatocytes that simultaneously undergo both gluconeogenesis and *de novo* lipogenesis. These dual-positive hepatocytes were also present in human hepatocytes from humanized mouse livers. Moreover, the number of dual-positive hepatocytes increased in high-fat diet-fed mice, suggesting a paradigm shift in our understanding of how the liver becomes insulin resistant.

INTRODUCTION

The mammalian liver is composed of parenchymal (hepatocytes) and non-parenchymal (endothelial, Kupffer, cholangiocytes, stellate) cells organized into repetitive hexagonal arrays termed lobules[1,2]. Within each lobule the hepatocytes are distributed from the portal triad (portal vein, hepatic artery, bile duct) at the six vertices and the central vein located at the centroid of the hexagon. The hepatocytes aligned within a lobule display functionally distinct metabolic properties and are generally

55 divided into three zones: the periportal hepatocytes (zone 1), midlobular hepatocytes
56 (zone 2) and the pericentral hepatocytes (zone 3), with emerging single-cell studies
57 indicating that hepatic zonation exists along a more continuous and finely partitioned
58 spectrum[3,4]. The pericentral hepatocytes display higher rates of glycolysis, bile acid and
59 glutamine biosynthesis[1,2]. The periportal hepatocytes are primarily responsible for beta-
60 oxidation and urea oxidation and in particular, gluconeogenesis[1,2]. However,
61 gluconeogenesis is a dynamic process that is regulated by numerous hormonal, neural
62 and metabolic inputs. During early states of fasting *in vivo*, we found that periportal
63 hepatocytes are initially responsible for gluconeogenesis, but as fasting duration
64 increased, the mid-zone and then pericentral hepatocytes underwent increased
65 gluconeogenic gene expression, protein levels and ultimately gluconeogenic activity that
66 approached that of the periportal hepatocytes[5]. In contrast, lipogenic gene expression
67 that is high in the fed state is rapidly downregulated to essentially undetectable levels
68 during the initial time frame of fasting induction. These data demonstrate the remarkable
69 plasticity of hepatocyte gluconeogenic gene expression and gluconeogenic activity
70 across the liver lobule depending upon organismal nutrient state.
71 While it is generally accepted that *de novo* lipogenesis is activated in the fed state
72 whereas gluconeogenesis and hepatic glucose output are activated in the fasted state,
73 several studies observed a measurable rate of gluconeogenesis and hepatic glucose
74 production in the fed state, despite the availability of dietary glucose[6,7]. Although not
75 thoroughly investigated, the molecular and cellular bases for the basal rate of hepatic
76 gluconeogenesis and hepatic glucose output was generally thought to represent
77 glucose production for the indirect pathway of glycogen synthesis[8-11].

78 In this study, we used a variety of single cell technologies to confirm the presence of
79 basal liver gluconeogenic activity transcriptionally and functionally in the fed state that
80 results in hepatic glucose release. Importantly, our data revealed that this basal
81 gluconeogenesis results from a subset of unique hepatocytes that simultaneously
82 display expression of both *de novo* lipogenic and gluconeogenic genes exclusively
83 localized to the periportal region. Spatial metabolomic imaging further confirmed that
84 this subset of periportal hepatocytes is capable of simultaneously undergoing both
85 gluconeogenesis and *de novo* lipogenesis, and have high rates of ATP turnover,
86 consistent with the energetic need to sustain these dual processes. Furthermore,
87 euglycemic-hyperinsulinemic clamps and PrimeFlow analyses suggested that these
88 hepatocytes are resistant to insulin suppression of gluconeogenic gene expression,
89 demonstrating natural insulin resistance under normal physiological conditions.
90 Moreover, the number of these naturally insulin-resistant hepatocytes is increased by
91 high-fat diet feeding.
92

93 **RESULTS**

94 **Gluconeogenic genes are transcribed in hepatocytes in the fed state**

95 To investigate the regulation of liver gene expression in the normal physiological
96 transitions between fed and fasted states, we used a previously established protocol in
97 which mice rapidly consume food and fill their stomachs to create a relatively uniform
98 fed state, and following food removal, facilitate a uniform transition into the fasted
99 state[5,12]. We first confirmed our previous findings that lipogenic gene *Fasn* mRNA is
100 highly expressed in the fed state of total primary isolated hepatocytes and nearly

101 completely suppressed in the fasted state (Fig. 1A). In contrast to lipogenic gene
102 mRNA, the gluconeogenic gene *Pck1,* was highly expressed in the fasted state, yet
103 surprisingly there was a low but readily detectable mRNA in the fed state as well (Fig.
104 1B). There were no significant effects of fasting/feeding on the expression of
105 constitutively expressed gene albumin (*Alb*) mRNA (Fig. 1C). To determine if the
106 observed feeding state changes in mRNA levels were due to a transcriptional process,
107 we examined the transcriptional activation of lipogenic and gluconeogenic genes by
108 performing DNA-dependent RNA polymerase II (RNAPII) ChIP-seq to assess RNAPII
109 gene occupancy in total primary isolated hepatocytes. As expected, RNAPII occupancy
110 was relatively high across the gene body of *Fasn* in the fed state with very low binding
111 in the fasted state (Fig. 1D). RNAPII occupancy on other lipogenic genes *Acly* and
112 *Elovl6*, displayed a similar pattern (Fig. S1A and S1B). Both *Fasn* and *Acly* displayed a
113 peak of RNAPII at the transcription start site indicative of proximal promoter pausing[13].
114 In contrast, the gluconeogenic genes *Pck1* and *G6pc* showed the opposite trend with
115 higher RNAPII occupancy in the fasted state. Although both *Pck1* (Fig. 1E) and *G6pc*
116 (Fig. S1C) displayed strong gene occupancy by RNAPII in their active (fasted) state, we
117 also observed RNAPII gene occupancy in the inactive fed state. In addition, there was
118 no evidence of proximal promoter pausing for the gluconeogenic genes. In contrast,
119 there were no changes in RNAPII occupancy for *Alb* (a constitutive hepatocyte gene,
120 Fig. 1F). As a control, the *Ins1* gene, which is not expressed in hepatocytes, showed
121 virtually no RNAPII occupancy in either the fed or fasted state (Fig. 1G).
122 The apparent transcription of gluconeogenic genes in the fed state could occur in all
123 hepatocytes or be restricted to a subset of hepatocytes. To explore these possibilities,

124 we isolated pericentral and periportal hepatocytes from fed and 16 h fasted mice using
125 a digitonin ablation method that we modified for application in mice[5,14,15]. The isolated
126 pericentral (PC) and periportal (PP) hepatocytes were then subjected to RNAPII ChIP-
127 seq analyses. To confirm the relative purity of separation we examined the mRNA
128 expression levels of *Cyp2e1*, an established PC hepatocyte marker, and *Cyp2f2*, an
129 established PP marker[3,5,16]. As shown in Figure S2A there was a ~ 6 to 9-fold
130 enrichment of *Cyp2e1* in the PC hepatocytes and an ~ 4 to 6-fold enrichment of *Cyp2f2*
131 in the PP hepatocytes (Fig. S2B).
132 RNAPII ChIP-seq demonstrated that *Fasn* gene was transcriptionally active in both
133 the PC and PP hepatocytes in the fed state, although somewhat greater in the PP
134 hepatocytes (Fig. S2C). The *Fasn* gene occupancy of RNAPII in both PC and PP
135 hepatocytes is consistent with the mRNA expression of lipogenic genes levels across
136 the liver lobule[5]. In any case, in the fasted state there was essentially no RNAPII
137 occupancy of *Fasn* gene in either PC or PP hepatocytes with the proximal promoter
138 pausing peak readily observable in both zones. As expected in the fasted state, RNAPII
139 occupancy of the *Pck1* gene was high in both the PC and PP hepatocytes (Fig. S2D),
140 consistent with *Pck1* mRNA expression that is also expressed in both PC and PP
141 hepatocytes following long-term fasting[5]. However, in contrast to *Fasn* gene, in the fed
142 “off-state” *Pck1* gene still displayed substantial RNAPII occupancy in the PP
143 hepatocytes but nearly background levels in the PC hepatocytes (Fig. S2D). As
144 controls, RNAPII occupancy of *Alb* was neither zonated nor responsive to
145 fasting/feeding (Fig. S2E) and the RNAPII tracks for *Ins1* was essentially background

146 (Fig. S2F). These data indicate that the basal (fed state) transcription and expression of
147 gluconeogenic genes occur predominantly in PP hepatocytes.
148
149 **Lipogenic and gluconeogenic genes are co-expressed in a subset of periportal**
150 **hepatocytes**
151 We next addressed whether all PP hepatocytes or a subset of PP hepatocytes were
152 responsible for the basal expression of gluconeogenic genes in the fed state. To
153 address this, we first utilized quantitative targeted single cell RNA-seq (targeted scRNA-
154 seq) using the 10x genomic platform for a selective subset of metabolic genes[5]. Cell
155 ranger and Loupe Browser were used for analyses for the quantitative targeted scRNA-
156 seq to establish UMAP cluster maps of the hepatocytes in the fully fed and fasted states
157 (Fig. 2A). To identify the position of the PC and PP hepatocytes (Fig. 2B) we took
158 advantage of previous studies that have characterized the localization of specific
159 zonation markers[3,5,16]. As examples, the PC markers *Cyp2e1* and *Gulo* (Fig. 2C) were
160 highly colocalized to one region whereas the PP markers *Cyp2f2* and *Hsd17b13* (Fig.
161 2D) were highly colocalized to another distinct region. As these genes are typically
162 expressed as a gradient across the lobule, (with the notable exception of *Glul* that is
163 highly restricted to hepatocytes in one to two layers around the central vein), the other
164 lower expressing cells likely represent the mid-zone hepatocytes[1,5]. As expected, in the
165 fully fed state, the *de novo* lipogenic gene *Fasn* was found in both the PC and PP
166 hepatocytes but following fasting was essentially absent from all the hepatocytes (Fig.
167 2E). On the other hand, the gluconeogenic gene *Pck1* was expressed in both the PC
168 and PP hepatocyte clusters in the fasted state, but also showed expression in a subset

169 of PP, but not PC, hepatocytes in the fed state (Fig. 2F). Alignment of the UMAPs for
170 the hepatocytes that co-express both *Fasn* and *Pck1* mRNA in the fed state indicated
171 they account for 7% of the periportal hepatocytes (Fig. 2G). In addition, comparison of
172 other core *de novo* lipogenic genes (*Acly*, *Acaca*, and *Elvol6*) with the gluconeogenic
173 gene *G6pc* also demonstrated that approximately 19% of PP hepatocytes
174 simultaneously co-expressed these mRNAs (Fig. S3A-E).
175

176 **_Fasn_ and _Pck1_ are actively co-transcribed in a subset of periportal hepatocytes**

177 To confirm the scRNA-seq identification of a periportal hepatocyte subset that
178 simultaneously expresses both gluconeogenic and *de novo* lipogenic genes, we utilized
179 Hybridization Chain Reaction RNA Fluorescence *in Situ* Hybridization (HCR RNA-FISH)
180 to simultaneously visualize the transcription sites (TS) of the *Fasn* and *Pck1* genes.
181 Simultaneous glutamine synthetase RNA-FISH was used to identify the PC region
182 (Figure 3, *Glul* not shown)[1,5]. In the fed state *Fasn* TS were readily observed throughout
183 the lobule but fewer *Pck1* TS were detected in a subset of the PP but not PC
184 hepatocytes (Fig. 3A, Fig. S4A and S4B). Magnified images clearly demonstrated the
185 presence of both *Fasn* and *Pck1* TS simultaneously in the same nucleus in a subset of
186 the PP hepatocytes (Fig. 3B). Quantification indicated that 24 % of the periportal
187 hepatocytes and 1 % of the pericentral hepatocytes displayed TS for both *Fasn* and
188 *Pck1* in the fed state (Fig. 3C). On the other hand, in the fasted state, *Pck1* TS was
189 readily detected throughout the lobule but with essentially no *Fasn* TS (Fig. 3D, Fig.
190 S4C and S4D). Magnified images of TS in the fasted state are shown in Fig. 3E.
191 Quantification indicated that hepatocytes that were dual-positive of TS were not

192 detected (Fig. 3F). These data directly demonstrate that the subset of PP hepatocytes
193 actively transcribed both lipogenic (*Fasn*) and gluconeogenic (*Pck1*) genes at the same
194 time.
195
196 **Periportal hepatocytes have basal pyruvate-to-glucose flux in the fed state**
197 Gene transcription and mRNA expression does not necessarily indicate functional
198 activity; we therefore directly determined the relative *de novo* lipogenesis and
199 gluconeogenesis activities by quantifying the fractional incorporation of $^{2}H_2O$ into
200 palmitate and [2,3-$^{13}C_2$] pyruvate into glucose (Fig. 4). As expected, the fractional
201 amount of ^{2}H-palmitate in total hepatocytes from the fed state was substantially higher
202 (16-fold) compared to hepatocytes from the fasted state (Fig. 4A). The decomposition of
203 this overall palmitate enrichment is shown as the increased fed vs. fasted isotopologue
204 enrichment distribution (Fig. 4B). This large increase appears to result from the very low
205 fractional synthesis in the fasted state. Conversely, the average ^{13}C incorporated per
206 molecule of glucose synthesized was higher (2.4-fold) in the hepatocytes from the
207 fasted state compared to the fed state (Fig. 4C). The decomposition of the isotopologue
208 distribution of glucose is shown in Figure 4D with the majority of glucose isotopologues
209 synthesized as either M2- or M4-glucose. To address the potential zonation of both
210 glucose and palmitate synthesis, we next examined the relative synthesis rates in
211 isolated PC and PP hepatocytes.
212 Consistent with *Fasn* gene expression, *de novo* lipogenesis activity is relatively high
213 in the fully fed state (Fig. 4E) with very low activity in the fasted state and exhibits
214 similar levels between PC and PP hepatocytes. The fold stimulation from the fasted “off”

215 state and the active fully fed “on” state is approximately 30-fold in PC and 55-fold in PP
216 hepatocytes. The isotopologue distribution of palmitate is shown in Figure 4F. In
217 contrast, in the fed state there is a low level of gluconeogenesis from isolated PC
218 hepatocytes, but it is several-fold higher in the PP hepatocytes (Fig. 4G). In the fasted
219 state, both PC and PP hepatocytes display a higher rate of gluconeogenesis.
220 Importantly, the PC hepatocytes increase their gluconeogenic activity ~10-fold, whereas
221 the PP hepatocytes only increase their gluconeogenic activity ~4-fold due to the higher
222 basal activity (Fig. 4G). The isotopologue distribution of glucose is shown in Figure 4H,
223 which again shows mainly the formation of M2- and M4-glucose. These data
224 demonstrate that in the fed state, PP hepatocytes display a significant degree of
225 gluconeogenic activity, consistent with the PP expression of gluconeogenic genes in the
226 fed state. On the other hand, PC hepatocytes exhibit a metabolic plasticity which
227 enables them to become equally gluconeogenic in the fed to fasted transition.
228

229 **Dual-positive hepatocytes are insulin resistant in suppression of *Pck1***

230 Since the fed state is a normal physiologically anabolic state primarily driven by
231 insulin, the expression of *Pck1* in the fed state suggests that this subset of PP
232 hepatocytes was less responsive to insulin (i.e., insulin resistant), at least to insulin
233 suppression of *Pck1* gene expression and gluconeogenic activity. To address this, we
234 established a quantitative assay to isolate these dual expression (*Fasn* and *Pck1*)
235 hepatocytes using PrimeFlow that is a combination of *in situ* hybridization coupled with
236 flow cytometry[17]. As shown in Figure S5A hepatocytes are relatively large cells with a
237 broad forward (FSC-A) and side scatter (SSC-A) parameters. Primary hepatocytes also

238 display background fluorescence in the APC-Cy7 and mCherry channels, which were
239 used for the *Pck1* and *Fasn* fluorescent mRNA probes (Fig. S5B). Nevertheless, in the
240 fed state there is a substantial increase in the *Fasn* signal, resulting in 75 % of
241 hepatocytes positive for *Fasn* (Fig. S5C). Similarly, in the fasted state there is a
242 substantial increase in the *Pck1* signal with 71 % of the hepatocytes positive for *Pck1*
243 (Fig. S5D). Having established this gating range, when we co-label the fed state
244 hepatocytes with both the *Pck1* and *Fasn* probes and identified that approximately 12%
245 of the hepatocytes were dual-positive (Fig. S5E). With a quantitative method in hand,
246 we determined the number of dual *Pck1*/*Fasn* positive hepatocytes relative to the single
247 positive and dual negative hepatocytes and performed euglycemic-hyperinsulinemic
248 clamps in the 24-hour fasted state and the fed state at various insulin infusion rates. We
249 also determined the relative suppression of the *Pck1* and *G6pc* mRNA in total
250 hepatocytes. Under these conditions, the fasted *Pck1* and *G6pc* mRNA expression
251 levels significantly decreased at 0.3 mU/kg/min (Fig. S5F and S5G). In contrast, fed
252 *Pck1* mRNA in the dual-positive hepatocytes was not suppressed until 2 mU/kg/min of
253 infused insulin (Fig. S5H). These data directly demonstrate that the *Fasn*/*Pck1* dual-
254 positive hepatocytes are transcriptionally insulin resistant compared to the bulk liver
255 hepatocytes.
256 Together these findings demonstrate that a subset of PP hepatocytes simultaneously
257 express both gluconeogenic and lipogenic genes in the fed state (Figs. 2, 3, S3 and
258 S4), and that isolated PP hepatocytes can also display both gluconeogenic and *de novo*
259 lipogenic activities in the fed state (Fig. 4). However, this data does not directly
260 demonstrate that individual dual-positive hepatocytes are in fact dual functional. To test

261 for this possibility, we employed single cell spatial metabolic imaging to simultaneously
262 assess both gluconeogenic and *de novo* lipogenic activities within individual
263 hepatocytes
264
265 **A subset of liver regions has higher ATP turnover in the fed state**
266 Depending upon the substrate, gluconeogenesis requires 6-10 ATP molecules per
267 molecule of glucose generated. Similarly, synthesis of palmitate from acetyl-CoA
268 requires 7 ATP and 14 NAPDH molecules. Thus, if a single hepatocyte is
269 simultaneously engaged in both gluconeogenesis and *de novo* lipogenesis, it can be
270 hypothesized that there must necessarily be a high rate of ATP turnover compared to
271 the other bulk hepatocytes. During the process of energetic addition of phosphates to
272 nucleotides or metabolites, there is an exchange of the oxygen in the phosphate with
273 the oxygen in cell water[18-21]. ATP turnover reflects the percentage of ^{16}O in ATP
274 replaced by ^{18}O after the *in vivo* administration of ^{18}O-labeled water, reflecting whole
275 cell energetics, as the exchange of ^{18}O in high energy phosphates includes ATP
276 synthesis and ATP hydrolysis, and the ^{18}O can also be exchanged with creatine kinase
277 and adenylate kinase catalyzed phosphotransfer[22,23] (Table S1). Thus, we treated mice
278 with or without ^{18}O labeled water *in vivo* coupled with spatial imaging by DESI-Cyclic
279 IMS TOF. Figure 5 shows liver sections from the fed and 24 h fasted state that were
280 either untreated (unlabeled) or treated with ^{18}O labeled water as we previously reported
281 [23]. Mass spectrometry imaging was done at 60x60 μm for the mass of normally
282 abundant m0 (unlabeled) AMP in the negative ion mode. As mouse hepatocytes are
283 polygonal and are nominally 20-30 μm in diameter, this resolution likely reflects the

284 combination of several cells[24]. Regardless, the relative amount of the m0 AMP indicated
285 a relatively low signal in the fed state but was markedly increased in the fasted state,
286 indicating a greater turnover of AMP in the fasted state (Fig. 5A). In contrast, imaging
287 for ^{18}O-labeled AMP (m0+2 AMP) demonstrated an increased signal from background
288 in both the fasted and fed states, from the mice treated with ^{18}O labeled water
289 compared to control mice livers (Fig. 5B). More importantly, the liver cross-section in the
290 fasted state showed increased intensities suggesting increased turnover relative to the
291 fed state (Fig. 5B). In contrast, m0+2 ADP fasted and fed intensities were similar over
292 each slice, suggesting turnover was similar between the fed and fasted state. The
293 increase of m0+2 ATP intensities over the liver cross-section suggested turnover was
294 increased in the fed state compared to the fasted state, which would correspond to an
295 increase in ATP generation in the fed state (Fig. 5C). As these AMP, ADP and ATP
296 measurements were done on the same slice, m0+2 ADP and m0+2 ATP pixel densities
297 can be compared to m0+2 AMP in fed state with multiple sites of overlap between m0+2
298 AMP, ADP and ATP (Fig. 5D). These results revealed several discrete pixels that
299 clearly overlapped between m0+2 AMP (red), ADP (blue) and ATP (green) (Fig. 5D).
300 The white areas indicate pixel regions with strong overlap for all three signals. These
301 data strongly indicate that a small subset of liver regions have higher rates of ATP, ADP
302 and AMP turnover in the fed state, indicating increased energetics, which might be
303 expected for Dual-Modal hepatocytes.
304
305 **A subset of hepatocytes is lipogenic and gluconeogenic**

306 To more specifically address whether an individual hepatocyte can simultaneously
307 undergo both *de novo* lipogenesis and gluconeogenesis, we next utilized metabolic
308 spatial imaging to identify the formation of m0+4 palmitate (*de novo* lipogenesis) and
309 m0+3 glucose-6-phosphate (gluconeogenesis) from a liver section of mice *in vivo* fed
310 with U[^{13}C]-glucose. m0+3 glucose-6-phosphate (3 labeled carbons) can only be formed
311 from U[^{13}C]-glucose (6 labeled carbons) when the m0+6 glucose is metabolized to a
312 m0+3 triose. The triose then goes up the gluconeogenic pathway to glucose or first
313 down the glycolytic pathway into the TCA cycle and then back up the glycolytic pathway
314 to form glucose (Fig. 6A). On the other hand, labeled palmitate can only be formed if the
315 U[^{13}C]-glucose becomes m0+3 pyruvate and then enters the TCA cycle through
316 pyruvate dehydrogenase to generate the 2-carbon labeled acetyl-CoA. Subsequent
317 metabolism and addition of these 2-carbon labeled units for fatty acid synthesis results
318 in the formation of m0+2, m0+4 etc. labeled palmitate (Fig. 6A). The dual-imaging of
319 m0+4 palmitic acid (red) and m0+3 glucose-3-phosphate (blue) by DESI MSI at 25 x 25
320 μm demonstrated the presence of pixels that were dual positive for both (pink, indicated
321 by arrows) (Fig. 6B). The same experiment was performed with MALDI MSI in a lower
322 magnification (50 x 50 μm). The ingestion of U[^{13}C]-glucose in the fed state resulted in
323 the appearance of m0+4 palmitate acid (red) and m0+3 glucose-6-phosphate (blue)
324 throughout the liver section whereas there was no detectable background labeling when
325 ingestion of unlabeled glucose in a parallel mouse (Fig. 6C). A higher magnification of
326 this MALDI image showed the presence of pixels that were dual positive for both m0+4
327 palmitic acid and m0+3 glucose-6-phosphate (pink, indicated by arrows) (Fig. 6D).
328 Since this resolution does not provide single cell information[24], we next performed mass

329 spectrometry spatial imaging at 10 μm resolution for m0+4 palmitic acid (red) and m0+3
330 glucose-6-phosphate (blue) that we co-registered with H&E staining (Fig. 6E and F). As
331 is apparent, in this imaging each pixel is smaller than the hepatocytes and with a high
332 probability it represents a single hepatocyte (Fig. 6E and F). Consistent with the lower
333 resolution image, individual hepatocytes mostly display *de novo* lipogenesis in the fed
334 state (m0+2 palmitic acid positive, red) with fewer hepatocytes positive for m0+3
335 glucose-6-phopshate (blue). However again, there were several pixels in the field that
336 are dual positive (pink), consistent with the overlap seen with ATP, ADP and AMP
337 turnover (Fig. 5) and the dual-positive hepatocytes present as measured by both
338 scRNA-seq and PrimeFlow. As these data confirm the metabolic functional duality
339 (simultaneous gluconeogenic and *de novo* lipogenic activities), we have termed these
340 as Dual-Modal hepatocytes.
341
342 **Humanized mouse liver has dual-positive spots**
343 Having established the presence of hepatocyte subsets that simultaneously express
344 both *Fasn* and *Pck1* mRNA in the fed state of mouse liver, we addressed whether dual-
345 positive hepatocytes are also present in human liver hepatocytes. As patient surgical
346 interventions can only be performed in the fasted state, it is not possible to obtain liver
347 specimens or biopsy samples from humans in the fed state. Thus, we utilized a
348 humanized mouse model in which human hepatocytes replace greater than 95 % of the
349 mouse hepatocytes and performed 10x Genomics spatial transcriptomics Visium
350 analyses on liver sections[25].Similar to the mice data, RT-qPCR for human *Fasn* showed
351 relatively low expression in the fasted state with induction in the fed state (Fig. S6A).

352 Additionally, the human *Fasn* PCR primers were unable to detect *Fasn* mRNA in wild-
353 type mouse liver, indicating no cross-reactivity. Similarly, the human *pck1* PCR primers
354 did not cross-react with mouse *Pck1* but clearly displayed the fasted state induction of
355 *Pck1* (Fig. S6B). As the Visium protocol requires a prior fixation step, we also confirmed
356 that this fixation step did not disrupt the integrity of mRNA detection by RT-qPCR (Fig.
357 S6C and D). Relative differences in the expression of the human PC marker (*CYP1A2*)
358 and PP marker (*HSD17B13*) as shown in the violin plots (Fig. S6E and S6F) enabled
359 the identification of PC spots (blue) and PP spots (red) (Fig. S6G). The violin plots for
360 *Fasn* (Fig. S6H) and *Pck1* (Fig. S6I) display the expected zonation, in particular the
361 *Pck1* mRNA in the PP hepatocytes are elevated compared to those of the PC
362 hepatocytes. The distribution of the *Fasn*/*Pck1* dual-positive spots is marked in yellow
363 with the H&E staining of the section (Fig. S6J) and with a magnified region show in
364 Figure S6K. Quantification showed 9% of the PP hepatocytes were *Fasn*/*Pck1* dual-
365 positive (Fig. S6L). These results suggest Dual-Modal hepatocytes presumable exist in
366 human hepatocytes as well.
367
368 **Dual-positive spots increase in high-fat diet fed mice liver**
369 Lastly, having established the Dual-Modal (*Fasn*/*Pck1* positive) hepatocytes that are
370 naturally insulin resistant (Fig. S4) and are gluconeogenic in the fed state, we
371 speculated that in states of insulin resistance the number of these hepatocytes might
372 increase. To test this hypothesis, we determined the number of Dual-Modal hepatocytes
373 in mice fed a normal chow diet (NCD) or a high-fat diet for 3 months (3MHFD) and used
374 the Visium platform for spatial single dot analyses. t-SNE plots showed separation

375 between NCD and 3MHFD (Fig. S7A). Graph-based clustering showed zonation
376 patterns in both NCD and 3MHFD (Fig. S7B, S7C). Based on analyses of several
377 zonation markers such as *Cyp2e1* and *Glul* for pericentral (Fig. S7D) and *Cyp2f2* and
378 *Hsd17b13* for periportal (Fig. S7E), we identified the PC (pink) and PP (blue) spots in
379 the t-SNE plot, showing clear separation (Fig. S7F). The PC and PP regions in
380 comparison with histological H&E staining are shown in Figure 7A. The presence of lipid
381 droplets in the HFD fed mice that are specifically localized to the PC hepatocytes is
382 readily observed in the magnified region shown in Figure 7B, consistent with the known
383 zonation of triglyceride accumulation[26]. The distribution of zonation markers as violin
384 plots is shown in Figures 7C and 7D. As expected for the fed state, *Fasn* mRNA was
385 expressed in both PC and PP hepatocytes in both the NCD and 3MHFD fed mice (Fig.
386 S7G). Consistent with our previous findings, *Pck1* mRNA was also present in a subset
387 of periportal hepatocytes (Fig. S7H) that overlapped with the *Fasn* dots (Fig. S7G). The
388 overlap of *Fasn* and *Pck1* mRNA positive dots in the NCD and HFD fed mice is shown
389 in Figures 7E. Quantification of the number of dots that were dual positive was
390 approximately 4 % under NCD diet but following 3 months of HFD the number of dual
391 positive dots increased to approximately 13 % (Fig. 7F). Moreover, these overlapping
392 dots primarily occurred in the PP region (Fig. 7G). These data demonstrate that long
393 term HFD results in an increase in the number of the Dual-Modal (*Fasn*/*Pck1* positive)
394 hepatocytes.
395
396 **DISCUSSION**

397 Gluconeogenesis is a fundamental metabolic process in which non-carbohydrate
398 carbon substrates such as lactate, glycerol and amino acids are used to generate
399 glucose[2,27]. In mammals' gluconeogenesis is primarily performed in the hepatocyte,
400 although kidney and intestine cells are capable of driving significant gluconeogenesis as
401 well[27-29]. In general, gluconeogenesis is inhibited in the fed state when plasma glucose
402 levels rise as a result of dietary absorption, and insulin secretion is stimulated. In the
403 fasted state, dietary derived plasma glucose levels decline, reducing insulin secretion
404 and stimulating glucagon and epinephrine release to activate hepatic gluconeogenesis
405 and glucose release to restore and maintain a normal glycemic state. Two of the key
406 gluconeogenic enzymes phosphoenolpyruvate carboxykinase (gene *Pck1*) and glucose
407 6-phosphate catalytic subunit (gene *G6pc*) are not thought to be allosterically regulated,
408 but acutely controlled at the level of gene expression through upstream transcription
409 factors that are activated by protein kinase A (i.e., CREB, HNF4α, FoxO1) signaling and
410 suppressed by insulin signaling[27].
411 Despite this generalized regulation of hepatic gluconeogenic gene expression and
412 gluconeogenic activity in the fed and fasted states, previous studies assessing
413 gluconeogenesis observed a basal level of glucose production from the liver even in the
414 fed state[6,7]. In fact, examination of numerous hyperinsulinemic-euglycemic clamp data
415 clearly shows that an insulin suppression of hepatic glucose production is never
416 zero[30,31]. This has been typically ignored and assumed to simply represent a
417 background signal. Our data suggest otherwise, as the mRNA expression and
418 transcription of lipogenic genes are essentially zero in their respective off-state (fasted),
419 whereas there is always a measurable level of gluconeogenic gene expression,

420 transcriptional activation and gluconeogenic activity in their respective off-state (fed).
421 This fed state mRNA expression of *Pck1* was confirmed by multiple, independent
422 methodologies, including targeted quantitative single cell RNAseq, smFISH, HCR RNA-
423 FISH and PrimeFlow. Moreover, PrimeFlow demonstrated the presence of both mRNA
424 for *Fasn* and *Pck1* in the same cells and HCR RNA-FISH clearly visualized the same
425 nuclei displaying transcription sites for both *Fasn* and *Pck1*. Each of these assays
426 indicated a subset of periportal hepatocytes is dual *Fasn* and *Pck1* positive in the fed
427 state.

428 Hepatocyte zonation is well established as a property of regionally distinct cellular
429 functions localized across the liver lobule, and studies in the 1980's using fasted rats
430 reported that there was a 2 to 3-fold bias of gluconeogenesis in isolated PP hepatocytes
431 relative to PC hepatocytes[14,32]. We also found an approximate 1.4-fold bias in
432 gluconeogenic activity and *Pck1* gene expression in PP versus PC hepatocytes of
433 fasted mice. However, analyses of gluconeogenic activity in the fed state, although
434 absolutely less than in the fasted state, was approximately 3.2-fold greater in PP versus
435 PC hepatocytes. In parallel, very few *Pck1* transcription sites and very low levels of
436 *Pck1* mRNA or protein were detected in fed PC hepatocytes compared to PP
437 hepatocytes. These data are consistent with a subset of PP hepatocytes being
438 responsible for the basal (fed state) level of gluconeogenesis. As such, we refer to this
439 hepatocyte subset as Dual-Modal (DM) hepatocytes.

440 The conversion of U[^{13}C]-glucose to m0+2- and m0+4-palmitate is generally
441 accepted as a direct measure of *de novo* lipogenesis that is readily detected by mass
442 spectrometry imaging[33]. However, spatial mass spectrometry imaging cannot detect

443 labeled glucose within a hepatocyte, as glucose is rapidly secreted. Instead, we
444 measured hepatocyte content of m0+3-glucose-6-phosphate derived from ingested
445 U[^{13}C]-glucose. In order for U[^{13}C]-glucose to generate m0+3-glucose-6-phosphate, the
446 U[^{13}C]-glucose must at minimum be converted by glycolysis or the pentose cycle into
447 the triose pool, which in turn can either enter the TCA cycle (pyruvate->oxaloacetate-
448 >PEP->triose-P pool) for gluconeogenesis/glyceroneogenesis, or the trioses glycerol-3-
449 phosphate and dihydroacetone phosphate recombine to form fructose-1,6-phosphate
450 and subsequently glucose-6-phosphate. Regardless of whether recycled glucose is
451 derived from the triose-P pool after traveling to the triose-P pool via glycolysis and the
452 TCA cycle or the pentose cycle and/or via the TCA cycle, our finding of the generation
453 of m0+3-glucose-6-phosphate from ingested U[^{13}C]-glucose demonstrates that in the
454 fed state, a subset of hepatocytes exhibits a simultaneous, bidirectional metabolic flow
455 up and down the glycolytic pathway. Our finding that isolated PP hepatocytes in the fed
456 state generate secreted glucose is consistent with a novel demonstration of
457 gluconeogenesis in the fed state.
458 However, these data do not rule out other metabolic pathways for the generation of
459 stable isotope labeled trioses. For example, the trioses could also contribute to
460 glyceroneogenesis that in the fed state are needed for the generation of the backbone
461 for triacylglycerol synthesis. Another more intriguing possibility is that the formation of
462 m0+3 glucose-6-phosphate in the fed state may account for previous observations
463 supporting an indirect pathway for glycogen synthesis[8-11]. After glycogen is depleted in
464 the fasted state, it can be re-synthesized in the fed state by the direct pathway (dietary
465 glucose converted to glucose-6-phosphate epimerized to glucose-1-phosphate that

466 generates UDP-glucose for direct addition to glycogen[9,11]. Alternatively, glucose but
467 also gluconeogenic substrates (i.e., amino acids) can be used to generate trioses by
468 cycling down the glycolytic pathway into the TCA cycling and then metabolized via
469 pyruvate carboxylase then PEPCK to generate triose-P which can then generate
470 glucose-6-phosphate that is then used for the re-synthesis of glycogen[8-11]. Additional
471 stable isotope flux analyses will be necessary to distinguish between these distinct
472 routes of carbohydrate flux in this unique hepatocyte subpopulation, and which likely are
473 not mutual exclusive.
474 While we observed that both normal mouse liver as well as humanized mouse livers
475 express naturally insulin resistant, Dual-Modal hepatocytes, their functions in systemic
476 physiology and pathophysiology remain to be determined. One possibility is that during
477 ingestion of ketogenic diets, glucose, although lowered, still needs to be produced. In
478 this case, Dual-Modal hepatocytes could provide a mechanism to maintain basal
479 glycemic levels necessary for survival. Pathophysiologically, high-fat diet induced insulin
480 resistance resulted in an increase in the number of Dual-Modal hepatocytes. This opens
481 up the intriguing possibility that the change in proportion of this unique hepatocyte
482 subpopulation may be an important component leading to hepatic insulin resistance.
483
484 **Limitations of the study**
485 While we have identified a subset of hepatocytes termed Dual-Modal hepatocytes
486 that could potentially explain the cause of hepatic insulin resistance based on an
487 increased number of Dual-Modal hepatocytes in high-fat diet fed mice, it is important to
488 recognize that these data do not distinguish between whether the number of Dual-

489 Modal hepatocytes increase due to proliferation of the pre-existing Dual-Modal
490 hepatocyte subpopulation and/or due to the development of insulin resistance in normal
491 hepatocytes. Future lineage tracing studies will be necessary to assess these two
492 possibilities. Also, this study does not molecularly address how an individual cell can
493 apparently undergo gluconeogenesis and *de novo* lipogenesis at the same time, as
494 these two metabolic pathways are generally assumed to be mutually exclusive with
495 each other. The three most likely possibilities are i) futile cycling throughout the parallel
496 glycolytic and gluconeogenic pathways for either periportal and/or pericentral
497 hepatocytes (dependent on degree of fasted or refed states) thereby allowing
498 substrates to flow in both directions; ii) relatively rapid oscillations between
499 gluconeogenesis and *de novo* lipogenesis, perhaps operant in Dual-Modal hepatocytes,
500 so that they are not actually occurring simultaneously; and iii) subcellular
501 compartmentalization of metabolic flux such that different regions or mitochondria within
502 an individual hepatocyte can undergo either gluconeogenesis or *de novo* lipogenesis.
503

504 **RESOURCE AVAILABLITY**

505 **Lead contact**

506 Further information and requests for resources and reagents should be directed to and
507 will be fulfilled by the lead contact, Junichi Okada (junichi.okada@einsteinmed.edu)

508 **Materials availability**

509 This study did not generate new unique reagents.

510 **Data and code availability**

511 Raw ChIP and fastq files were deposited in the National Center for Biotechnology
512 Information Gene Expression Omnibus database and are available under accession
513 numbers: GSE315776, GSE263419 (previously published targeted scRNA-seq data)
514 and GSE320372 (VISIUM). This study was conducted using only publicly available
515 software; no custom code was used.
516

517 **ACKNOWLEDGEMENTS**

518 We wish to acknowledge that the data presented in this manuscript was made possible
519 through the expertise of The Albert Einstein College of Medicine Genomics, Animal
520 Physiology, Flow Cytometry and Metabolomics Core Facilities. We are thankful to Floric
521 Slimani for the smallFish package, Licheng Wu for euglycemic-hyperinsulinemic clamp
522 studies, and Shiori Okada for data analysis. This study was supported by NIH grants
523 DK020541, DK110063, DK069861, GM007491, CA013330, AI179019, AA031412, and
524 the PhoenixBio R&D Grant.
525

526 **AUTHOR CONTRIBUTIONS**

527 JO, AL, MH, AMX, RR, SVL, TS, GJS, CE, RCS, YQ and IJK all assisted in the
528 experimental design, performance and analyses of the data presented, and writing of
529 the manuscript. LL and KS assisted in the experimental design, bioinformatic analyses
530 and editing of the manuscript. VLS, FY, MH, CE, KS and JEP supervised this project,
531 experimental design, interpretation of data and writing the manuscript.
532

533 **DECLARATION OF INTERESTS**

534 The authors declare no competing interests.

535

536 **FIGURE LEGENDS**

537 **Figure 1 *Pck1* is transcribed in hepatocytes in the fed state.** (A) Relative mRNA
538 levels of *Fasn* in fed/fasted total hepatocytes. (B) Relative mRNA levels of *Pck1* in
539 fed/fasted total hepatocytes. (C) Relative mRNA levels of *Alb* in fed/fasted total
540 hepatocytes. (D) RNAP II ChIP of *Fasn* in fed/fasted total hepatocytes. (E) RNAP II
541 ChIP of *Pck1* in fed/fasted total hepatocytes. (F) RNAP II ChIP of *Alb* in fed/fasted total
542 hepatocytes. (G) RNAP II ChIP of *Ins1* in fed/fasted total hepatocytes.

543

544 **Figure 2 *Fasn* and *Pck1* are co-expressed in a subset of periportal hepatocytes.**
545 (A) UMAP visualizations of the targeted scRNA-seq based on feeding conditions. (B)
546 UMAP visualizations based on zonation. (C) UMAP of PC zonation markers *Cyp2e1*
547 and *Gulo.* (D) UMAP of PP zonation markers *Cyp2f2* and *Hsd17b13.* (E) UMAP of *Fasn*
548 positive hepatocytes. (F) UMAP of *Pck1* positive hepatocytes (G) UMAP of dual-positive
549 hepatocytes.

550

551 **Figure 3 *Fasn* and *Pck1* are actively co-transcribed in a subset of periportal**
552 **hepatocytes.** (A) HCR RNA-FISH image of *Pck1* (magenta) and *Fasn* (green) with
553 DAPI-stained nuclei (blue) in the fed state (representative image shown). Lobules show
554 the central vein (CV) on the left and the portal vein (PV) on the right. (B) Magnified
555 images of nuclei in box in panel (A). Arrows show transcription sites (TSs) (green
556 arrow=*Fasn*, white arrow=*Pck1*, individual channel images of *Pck1* and *Fasn* are shown

557 in Figure S4A and S4B). (C) Quantitative analysis of TSs in the fed state. Lines connect
558 TS quantification between PC and PP within a lobule (N=21 lobules). Data are from 3
559 individual mice and are represented with different colors. Mean ± s.d. is indicated. *P*-
560 value was calculated by paired *t*-test, N.S. if not indicated. 627 PC nuclei, 632 PP nuclei
561 were analyzed, Scale bar, 20 um. (D) HCR-RNA FISH image of *Pck1* (magenta) and
562 *Fasn* (green) with DAPI-stained nuclei (blue) in the fasted state (representative image
563 shown). Lobules show the central vein (CV) on the left and the portal vein (PV) on the
564 right. (E) Magnified images of nuclei in box in panel (D). White arrows highlight Pck1 TS
565 (individual channel images of *Pck1* and *Fasn* are shown in Figure S4C and S4D). (F)
566 Quantitative analysis of TS in the fasted state. Lines connect TS quantification between
567 PC and PP within a lobule (N=21 lobules). Data are from 3 individual mice and are
568 represented with different colors. Mean ± s.d. is indicated. *P*-value was calculated by
569 paired *t*-test, N.S. if not indicated. 705 PC nuclei, 822 PP nuclei were analyzed, Scale
570 bar, 20 um.
571
572 **Figure 4 Periportal hepatocytes have basal pyruvate-to-glucose flux in the fed**
573 **state.** (A) *De novo* palmitate measurements using deuterated water in total hepatocytes
574 from fed (n=4) and fasted (n=4) mice. Data are presented as mean values; error bars,
575 s.d. Comparison between groups was made with unpaired, two-tailed Student's *t*-test
576 (***P < 0.001). (B) Fed and fast palmitate isotopologues derived from $^{2}H_2O$ in total
577 hepatocytes. (C) ΣM_n (average ^{13}C carbons per molecule) of glucose derived from [2,3-
578 $^{13}C_2$]-pyruvate in total hepatocytes from fed (n=3) and fasted (n=5) mice. Data are
579 presented as mean values; error bars, s.d. Comparison between groups was made with

580 unpaired, two-tailed Student's *t*-test (***P < 0.001). (D) Fed and fast glucose
581 isotopologues derived from [2,3-$^{13}C_2$]-pyruvate in total hepatocytes. (E) De novo
582 palmitate measurements using deuterated water in PC/PP hepatocytes from fed (n=4)
583 and fasted (n=4) mice. Data are presented as mean values; error bars, s.d. Comparison
584 between groups was made with unpaired, two-tailed Student's *t*-test (**P < 0.01). (F)
585 Fed and fast palmitate isotopologues derived from $^{2}H_2O$ in PC/PP hepatocytes. (G) ΣM_n
586 (average ^{13}C carbons per molecule) of glucose derived from [2,3-$^{13}C_2$]-pyruvate in
587 pericentral (PC) and periportal (PP) hepatocytes from fed and fasted mice (n=5 for PC,
588 n=6 for FastPP, n=7 for FedPP). Data are presented as mean values; error bars, s.d.
589 Comparison between groups was made with unpaired, two-tailed Student's *t*-test (***P <
590 0.001). (H) Fed and fast glucose isotopologues derived from [2,3-$^{13}C_2$]-pyruvate in
591 PC/PP hepatocytes.
592
593 **Figure 5 A subset of liver regions has higher ATP turnover in the fed state.** (A)
594 Representative DESI image of unlabeled AMP (M0) from unlabeled and 18O labeled
595 water intraperitoneal+gavage mice in the fed and fasted state. (B) Representative DESI
596 image of labeled AMP (m0+2) from unlabeled and 18O labeled water
597 intraperitoneal+gavage mice in the fed and fasted state. (C) Representative DESI image
598 of labeled ADP (m0+2) (left) and ATP-Na (m0+2) (right) from 18O labeled water
599 intraperitoneal+gavage mice in the fed and fasted state. (D) Representative DESI image
600 of labeled AMP (m0+2, red), ADP (m0+2, blue), and ATP-Na (m0+2, green) merged as
601 one image. The white areas indicate pixel regions with strong overlap for all three
602 signals.

603

604 **Figure 6 A subset of hepatocytes is lipogenic and gluconeogenic.** (A) Scheme of
605 detecting Dual-modal (DM) spots with U^{13}C glucose. (B) 25 x 25 μm DESI image of
606 U[^{13}C]-glucose labeled m0+4 Palmitic acid (red) and m0+3 Glucose-6-phosphate (blue);
607 pink represent the DM spots. White arrows highlight the DM spots. (C) Low
608 magnification MALDI image of U[^{13}C]-glucose labeled m0+4 Palmitic acid (red) and
609 m0+3 Glucose-6-phosphate (blue); pink represent the DM spots, unlabeled glucose
610 section as control. Each pixel is 50 μm. (D) High magnification MALDI image of U[^{13}C]-
611 glucose labeled m0+4 Palmitic acid (red) and m0+3 Glucose-6-phosphate (blue); pink
612 represent the DM spots. White arrows highlight the DM spots. Each pixel is 50 μm. (E)
613 High magnification of H&E staining. (F) High magnification MALDI image of U[^{13}C]-
614 glucose labeled m0+2 Palmitic acid (red) and m0+3 Glucose-6-phosphate (blue); pink
615 represent the DM hepatocytes. White arrows highlight the DM hepatocytes. Each pixel
616 is 10 μm.

617

618 **Figure 7 Dual-positive spots increase in high-fat diet fed mice liver.** (A) Spatial
619 transcriptomics image of Normal Chow Diet (NCD) fed mice and 3 Month High Fat Diet
620 (3MHFD) fed mice with Pericentral (PC)/Periportal (PP) spots highlighted. (B) A
621 representative lobule shown in a higher magnification with central vein (CV) on the left,
622 portal vein (PV) on the right. Pink spots are PP, blue spots are PC. (C) Violin plot of
623 *Cyp2e1* (pericentral (PC) marker) log normalized expression in PC/PP spots of NCD
624 and 3MHFD fed mice. (D) Violin plot of *Cyp2f2* (periportal (PP) marker) log normalized
625 expression in PC/PP spots of NCD and 3MHFD fed mice. (E) Distribution of DM spots in

626 NCD and 3MHFD fed mice; yellow spots show DM spots. (F) Quantification of DM spots
627 in NCD and 3MHFD fed mice. (G) Quantification of DM spots in PC/PP spots of NCD
628 and 3MHFD fed mice.
629
630 **Supplementary Figures**
631 **Figure S1 *G6pc* is transcribed in hepatocytes in the fed state.** (A) RNAP II ChIP of
632 *Acly* in fed/fasted total hepatocytes. (B) RNAP II ChIP of *Elovl6* in fed/fasted total
633 hepatocytes. (C) RNAP II ChIP of *G6pc* in fed/fasted total hepatocytes.
634
635 **Figure S2 *Pck1* is transcribed in periportal hepatocytes in the fed state.** (A)
636 Relative mRNA levels of *Cyp2e1* in in fed/fasted PC/PP hepatocytes. (B) Relative
637 mRNA levels of *Cyp2f2* in in fed/fasted PC/PP hepatocytes. RNAP II ChIP of *Fasn* in
638 fed/fasted PC/PP hepatocytes. (D) RNAP II ChIP of *Pck1* in fed/fasted PC/PP
639 hepatocytes. (E) RNAP II ChIP of *Alb* in fed/fasted PC/PP hepatocytes. (F) RNAP II
640 ChIP of *Ins1* in fed/fasted PC/PP hepatocytes.
641
642 **Figure S3 *Acly*, *Acaca*, *Elovl6*, and *G6pc* are co-expressed in a subset of**
643 **hepatocytes.** (A) UMAP of *Acly* positive hepatocytes. (B) UMAP of *Acaca* positive
644 hepatocytes. (C) UMAP of *Elovl6* positive hepatocytes. (D) UMAP of *G6pc* positive
645 hepatocytes.
646
647 **Figure S4 *Pck1* is actively transcribed in the fed state.** (A) HCR RNA-FISH image of
648 *Pck1* (magenta) with DAPI-stained nuclei (blue) in the fed state (representative image

649 shown). Lobules show the central vein (CV) on the left and the portal vein (PV) on the
650 right. (B) HCR RNA-FISH image *Fasn* (green) with DAPI-stained nuclei (blue) in the fed
651 state (representative image shown). Lobules show the central vein (CV) on the left and
652 the portal vein (PV) on the right. (C) HCR RNA-FISH image of *Pck1* (magenta) with
653 DAPI-stained (blue) in the fasted state (representative image shown). Lobules show the
654 central vein (CV) on the left and the portal vein (PV) on the right. (B) HCR RNA-FISH
655 image *Fasn* (green) with DAPI-stained (blue) in the fed state (representative image
656 shown). Lobules show the central vein (CV) on the left and the portal vein (PV) on the
657 right. Scale bar, 20 um.
658
659 **Figure S5 Dual-positive hepatocytes are insulin resistant in suppression of *Pck1.***
660 (A) Flow cytometry gating strategy utilizing FSC-A and SSC-A for size selection of
661 hepatocytes. (B) Background fluorescence of hepatocytes. (C) Gating of *Fasn* based on
662 fed hepatocytes. (D) Gating of *Pck1* based on fasted hepatocytes. (E) Representative
663 flow cytometry result of *Fasn*/*Pck1* in the fed state; the red quadrant shows the Dual-
664 modal (DM) hepatocytes. (F) Insulin suppression of *G6pc* mRNA expression based on
665 hyperinsulinemic-euglycemic clamps on fasted hepatocytes. (G) Insulin suppression of
666 *Pck1* mRNA expression based on hyperinsulinemic-euglycemic clamps on fasted
667 hepatocytes. (H) Insulin suppression of *Pck1* mRNA expression on DM hepatocytes
668 based on hyperinsulinemic-euglycemic clamps in the fed state.
669
670 **Figure S6 Humanized mouse liver has dual-positive spots.** (A) Relative mRNA
671 levels of human *Fasn* from fresh frozen liver tissue (mouse liver vs. humanized liver,

672 fed/fasted). (B) Relative mRNA levels of human *Pck1* from fresh frozen liver tissue
673 (mouse liver vs. humanized liver, fed/fasted). (C) Relative mRNA levels of human *Fasn*
674 from 4% PFA fixed liver sections (humanized liver). (D) Relative mRNA levels of human
675 *Pck1* from 4% PFA fixed liver sections (humanized liver). (E) Violin plot of *Cyp1a2* (PC
676 marker) log normalized expression. (F) Violin plot of *Hsd17b13* (PP marker) log
677 normalized expression. (G) Spatial Transcriptomics slide from fed mice with Pericentral
678 (PC)/Periportal (PP) spots highlighted. (H) Violin plot of *Fasn* (lipogenic gene) log
679 normalized expression. (I) Violin plot of *Pck1* (gluconeogenic gene) log normalized
680 expression. (J) Spatial Transcriptomics slide from fed mice with Dual-Modal (DM) spots
681 highlighted. (K) DM spots image with PC/PP alignment. (L) Percentage of DM spots in
682 PC/PP regions.
683
684 **Figure S7 t-SNE separates NCD and 3MHFD.** (A) t-SNE visualization of spatial
685 transcriptomics based on feeding conditions (Normal Chow Diet (NCD) and 3-Month
686 High-Fat Diet (3MHFD). (B) Spatial transcriptomics image of NCD fed mice and 3MHFD
687 fed mice with graph-based clustering highlighted. (C) t-SNE visualization of spatial
688 transcriptomics based on graph-based clustering. (D) t-SNE visualization of pericentral
689 markers *Cyp2e1* and *Glul*. (E) t-SNE visualization of periportal markers *Cyp2f2* and
690 *Hsd17b13*. (F) t-SNE visualization of spatial transcriptomics based on zonation. (G)
691 spatial transcriptomics image of *Fasn* positive spots in NCD and 3MHFD fed mice. (H)
692 spatial transcriptomics image of *Pck1* positive spots in NCD and 3MHFD fed mice.
693

694 **Table S1 Compendium of $^{18}O/^{16}O$ exchange reactions which determine ATP**

695 **turnover.**

696

697 **Table S2 Primer Sequences**

698

699 **METHODS**

700 **KEY RESOURCES TABLE**

REAGENT or RESOURCE	SOURCE	IDENTIFIER
Antibodies		
RNAPII subunit B1 (Rpb1) NTD	Cell Signaling	14958
Chemicals, peptides, and recombinant proteins		
Liberase	Sigma-Aldrich	5401127001
Digitonin	Sigma-Aldrich	D141-500MG
Percoll	Sigma-Aldrich	P4937-500ML
Critical commercial assays		
ChIP DNA Clean & Concentrator kit	Zymo Research	D5205
NEBNext® Ultra™ II DNA Library Prep Kit	New England Biolabs	E7645
HCR RNA-FISH	Molecular Instruments	V3.0 (N/A)
PrimeFlow RNA Assay Kit	Invitrogen	88-18005-204
Deposited data		
ChIP sequence	This paper, GEO	GSE315776
Targeted scRNA-seq	Okada et al[5], GEO	GSE263419
Visium (spatial transcriptomics)	This paper, GEO	GSE320372
Experimental models: Organisms/strains		
C57Bl/6J	The Jackson Lab	000664
Oligonucleotides		
Illumina® single Index Primers Set 1	New England Biolabs	E7335
Illumina® single Index Primers Set 2	New England Biolabs	E7500
See Table S2 for primer sequences	This paper	N/A
Software and algorithms		
Trim Galore	Krueger et al	https://github.com/FelixKrueger/TrimGalore, V0.6.7

Bowtie2	Langmead et al[34]	V2.4.5
Samtools	Li et al[35]	V1.6
DeepTools	Ramirez et al[36]	V3.5.1
Cell Ranger	10x Genomics	V6.0.1
Small Fish (Cellpose-SAM, big-fish)	Slimani et al	https://github.com/SmallFishGUI/small_fish_gui, V2.1.10
Space Ranger	10x Genomics	V2.0.0, V3.1.0
Other		
PicoLab Rodent Diet 20	LabDiet	5053
Rodent Diet with 60 kcal% Fat	Research Diets	D12492
Modified OSD with Macronutrient Content Similar to LabDiet 5053	Research Diets	D17011901px

701

702 **EXPERIMENTAL MODEL AND STUDY PARTICIPANT DETAILS**

703 **Animals**

704 All animal studies were conducted in accordance with protocols approved by the Albert
705 Einstein College of Medicine Institutional Animal Care and Use Committee (IACUC).
706 Unless otherwise indicated, experiments were performed using 10-14-week-old
707 C57Bl/6J wild-type male mice (The Jackson Laboratory, 000664). Spatial
708 transcriptomics studies were performed using 18-week-old mice. Animals were housed
709 in an IACUC-approved facility under ambient temperature and humidity with a 12-hour
710 light/dark cycle (lights turn on 7:00, lights turn off 19:00) and group housing. Mice had
711 free access to water and laboratory mouse chow diet (LabDiet, 5053), unless otherwise
712 specified. For high-fat diet studies, mice were fed a 60% fat diet (Research Diets,
713 D12492) beginning at 6 weeks of age for 3 months.
714 To align feeding conditions, mice were trained for 3 days to a time-restricted feeding
715 schedule by removing food at 17:00 and refeeding at 9:00 the following day (16-hour
716 fasting and 8-hour feeding) as previously described[5,12]. On the day of the experiment,

717 mice were provided food with drinking water supplemented with 20% sucrose (w/v) at
718 9:00. Fed mice were sacrificed at 13:00, corresponding to 4 hours of feeding. For fasted
719 mice, food and sucrose-containing water were removed at 13:00, drinking water was
720 replaced with regular water, and mice were fasted for 24 hours before sacrifice at 13:00
721 the following day. For pericentral/pericentral ChIP sequencing studies, mice were
722 sacrificed after 16 hours of fasting. For high-fat diet studies (and control mice), food was
723 removed at 7:00, refed at 19:00, and sacrificed at 23:00 (12-hour fasting and 4-hour
724 feeding).

725 **Humanized liver chimeric mice**

726 uPA SCID-based humanized liver chimeric mice were generated as previously
727 described and maintained with vitamin C containing chow diet (modified LabDiet 5053
728 containing 130 ppm vitamin C)[25]. Humanized liver chimeric mice were subjected to a
729 time-restricted feeding schedule modified to 10-hour fasting and 14-hour feeding.

730

731 **METHOD DETAILS**

732 **Hepatocyte Isolation**

733 Liver perfusion and hepatocyte isolation were performed under anesthesia as previously
734 described[5]. For total hepatocyte isolation, a catheter was placed in the portal vein (PV)
735 and the lower inferior vena cava (IVC) was cut for drainage. For zonated hepatocyte
736 isolation, catheters were placed in both the PV and IVC, and the perfusion line was
737 connected to the PV for periportal (PP) isolation of to the IVC for pericentral (PC)
738 isolation. Livers were perfused with pre-warmed PBS (42 °C) at 5 mL/min, then
739 switched to enzyme buffer solution (EBS, 15 mL) containing liberase (0.05 mg/mL)

740 (Sigma-Aldrich, #5401127001). For zonated hepatocyte isolation, 833 µL of 5-10mM
741 digitonin (Sigma-Aldrich, #D141-500MG) was injected via the unconnected catheter
742 (IVC for PP, PV for PC), after which the vessel was cut, and perfusion was immediately
743 resumed. Following perfusion, the liver was cut from the mouse and placed in cold
744 DMEM (without glucose) or Krebs-Henseleit (KH) buffer, gently dissociated, and filtered
745 through a 100 µm cell strainer. For liver hepatocyte purification, the cells were
746 centrifuged at 40 x *g* for 5 min at 4 °C, followed by Percoll (Sigma-Aldrich, #P4937-
747 500ML) solution (80 x *g* for 10 min at 4 °C), then washed by DMEM or KH buffer.
748 Hepatocytes were counted and assessed for viability prior to downstream applications.

749 **ChIP sequencing**

750 Fixation: Total hepatocyte (Fig. 1 and Fig. S1) and periportal/pericentral hepatocyte
751 (Fig. S2) isolation was performed on fasted and fed mice as described above with the
752 exception that all sample processing after liberase digestion was done using ice-cold
753 DBPS without calcium or magnesium (Gibco, #14190136) containing protease (Sigma,
754 #S8830) and phosphatase inhibitors (Sigma, #P5726) (referred to as DPBS buffer).
755 After final wash (see above), hepatocytes were resuspended in room temperature
756 DPBS buffer at concentration of 1 million cells/mL and formaldehyde (ThermoFisher,
757 #28908) was added to final concentration of 1%. Hepatocyte suspension was fixed at
758 room temperature for 10 min with gentle rolling. Fixation was stopped by adding glycine
759 in water (final concentration of 125 mM) containing protease and phosphatase
760 inhibitors, and hepatocytes were incubated for additional 15 min at room temperature
761 with gentle rolling. Hepatocytes were washed 1X in ice-cold DPBPS buffer, aliquoted in

762 Eppendorf tubes at 1 million cells per tube, pelleted/aspirated, and snap frozen in liquid
763 nitrogen for long-term storage at -80°C.
764 Immunoprecipitation: Immunoprecipitation reagents was prepared by washing Protein A
765 Dynabeads (ThermoFisher, #10002D) in chromatin dilution buffer (0.5% Triton X-100,
766 2mM EDTA, 20mM Tris, 150 mM NaCl in water) on DynaMag-2 (ThermoFisher,
767 #12321D) and combining with anti RNAPII subunit B1 (Rpb1) NTD rabbit monoclonal
768 antibody (Cell Signaling, #14958) at ratio of 630 µg Dynabeads to 4 µg antibody per IP
769 reaction. Dynabead-antibody mixture was pre-incubated at 4°C for 3 hours with gentle
770 rolling.
771 Sonication: Fixed-frozen hepatocyte pellets (1 million cells per IP reaction) were thawed
772 on ice and washed 1X with 500 µL cold DPBS buffer before resuspension in 500 µL
773 cold DPBS buffer with 0.5% Triton-X100 and incubation on ice for 10 min. Hepatocytes
774 were then centrifuged at 2600 xg for 5 min at 4°C, gently aspirated, and washed 1X with
775 500 µL cold tris-EDTA buffer (Sigma, #93283) containing 0.5% SDS (Sigma, #71736)
776 with protease/phosphatase inhibitors (TE-SDS buffer) before centrifuging again at 2600
777 xg for 5 min at 4°C. Supernatant was carefully aspirated, pellet was resuspended with
778 200 µL cold TE-SDS buffer, and sample was transferred to 1.5 mL Bioruptor Pico tubes
779 (Diagenode, #C30010016) on ice before sonication in 4°C water bath for 3 cycles (30
780 sec on / 30 sec off) with Easy Mode using Bioruptor Pico sonication device (Diagenode,
781 #B01080010). After sonication, sample was transferred back to 1.5 mL Eppendorf tubes
782 on ice and combined with 800 µL cold chromatin dilution buffer with
783 protease/phosphatase inhibitors (see above). Samples were centrifuged at 16,000 xg
784 for for 20 min at 4°C to remove debris and supernatant containing soluble chromatin

785 was transferred to new Eppendorf tubes on ice. DNA concentration across all samples
786 was checked using Qubit dsDNA HS kit (ThermoFisher, #Q33231) and normalized with
787 chromatin dilution buffer. For each sample, a 200 µL aliquot was collected as input and
788 a second aliquot (900 µL) was combined with 100 µL of Dynabead-antibody mixture,
789 briefly vortexed, and incubated overnight at 4°C with gentle rolling.
790 Washing: After overnight incubation, IP samples were washed in 4°C cold-room as
791 follows. Samples were placed on DynaMag-2 for 1 min, supernatant was removed and
792 discarded, 500 µL of pre-chilled wash buffer was added, and samples were rotated end-
793 over-end in cold-room for 5 min before repeating this process. Washes consisted of first
794 RIPA-140 (0.1% SDS, 1% Triton X-100, 1 mM EDTA, 10 mM Tris, 140 mM NaCl, 0.1%
795 sodium deoxycholate (Sigma, #D6750) in water), second RIPA-300 (0.1% SDS, 1%
796 Triton X-100, 1 mM EDTA, 10 mM Tris, 300 mM NaCl, 0.1% sodium deoxycholate in
797 water), third LiCl buffer (250 mM LiCl (Fisher Scientific, #L121), 0.5% Igepal ca-630 (MP
798 Biomedicals, # 198596), 1 mM EDTA, 10 mM Tris, 0.5% sodium deoxycholate in water),
799 fourth Tris-EDTA buffer (Sigma, #93283) with 0.2% Triton X-100, and fifth Tris-EDTA
800 buffer alone.
801 Elution: Wash buffer was removed, and chromatin was eluted from Dynabeads as
802 follows[37]. Briefly, 100 µL of elution buffer (1% SDS, 1 mM EDTA, 10 mM Tris in water)
803 was added to beads before vortexing and incubating at 65°C for 5 min followed by room
804 temperature incubation for 15min with vortexing every 5 min. Beads were placed on
805 DynaMag-2 for 1 min, and supernatant containing immunoprecipitated chromatin (~100
806 µL) was carefully collected and saved. Beads then underwent a second round of elution,
807 and the two supernatant collections were combined (~200 µL total).

808 RNase digestion, reverse cross-linking, and DNA purification: Input and IP samples
809 were combined with NaCl (final concentration of 160 mM) and RNase A (final
810 concentration of 20 µG/mL) (Roche, # 11119915001) and incubated at 65°C overnight
811 as previously outlined[37]. Afterwards, EDTA (final concentration of 5 mM) and proteinase
812 K (final concentration 200 µG/mL) (Invitrogen, # 100005393) were added, and samples
813 were incubated at 45°C for 2 h. Finally, input and IP DNA was purified using ChIP DNA
814 Clean & Concentrator kit (Zymo Research, #D5205) according to manufacturer's
815 guidelines, and DNA concentration was quantified using Qubit dsDNA HS kit. Fraction
816 of purified input DNA was run on agarose gel to assess fragmentation pattern (~100-
817 500 bp).
818 Library preparation, sequencing, and data processing: Library preparation was
819 performed using NEBNext® Ultra™ II DNA Library Prep Kit for Illumina® (New England
820 Biolabs, #E7645) according to manufacturer's guidelines with NEBNext® Multiplex
821 Oligos for Illumina® single Index Primers Set 1 and Set 2 (New England Biolabs,
822 #E7335 and #E7500). Premade libraries were sent to Novogene for sequencing using
823 NovaSeq paired-end sequencing at 150 base pairs per read (PE150). Raw fastq files
824 were first processed to remove adapter sequences and low-quality bases using Trim
825 Galore (v0.6.7) with "--stringency 5". Trimmed reads were then aligned to mm10
826 reference genome using bowtie2 (v2.4.5) with default parameters[34]. The resulting SAM
827 files were converted to BAM files using samtools (v1.6) view with "-f 2 -q 10"[35].
828 Duplicates were removed using samtools rmdup. Coverage tracks were generated
829 using the bamCoverage tool from the deepTools (v3.5.1) suite with the "--extendReads -
830 -normalizeUsing CPM" option[36]. Input normalization was performed using log2 ratio and

831 bin size set to 5 with bigwigCompare from deepTools. Normalized BigWig files were
832 visualized using Integrative Genomics Viewer (IGV)[38]. Total hepatocyte gene tracks
833 (Fig. 1 and Fig. S1) represent IP over input signal; periportal/pericentral hepatocyte
834 gene tracks (Fig. S2) represent IP signal alone since input signal was negligible in
835 previous experiments.

836 **RNA isolation and quantitative PCR (RT-qPCR)**

837 Total RNA isolation from isolated hepatocytes was done using the RNeasy mini kit
838 (Qiagen, #74106) in combination with TRIzol (Invitrogen, #15596026) according to the
839 manufacture's protocol. cDNA was synthesized using SuperScript IV VILO (Invitrogen,
840 #11756050) and RT-qPCR was performed using PowerUp SYBR Green Master Mix
841 (Applied Biosystems, #A25778) on a QuantStudio 6 system (Applied Biosystems).
842 Relative gene expression was determined by the ΔΔCt method and normalized to *Ppib*.
843 Primer sequences are listed in Table S2.

844 **Targeted Single-cell RNA sequencing (targeted scRNA-seq)**

845 To characterize dual-modal hepatocytes, we analyzed a publicly available targeted
846 single-cell RNA sequencing (scRNA-seq) dataset covering 61 specific genes[5]. The
847 panel consisted of pericentral and periportal hepatocyte markers, general parenchymal
848 and non-parenchymal cell markers, as well as genes involved in gluconeogenesis,
849 lipogenesis, bile acid synthesis, and several secreted hepatokines. Raw FASTQ files
850 were obtained from the NCBI Gene Expression Omnibus (GEO; accession no.
851 GSE263419). Gene expression levels were quantified using Cell Ranger (v.6.0.1; 10x
852 Genomics) in targeted gene expression mode. Positive cells were defined by applying

853 thresholds determined via ridge plot analysis and compared with RT-qPCR results as
854 previously described[5].

855 **HCR RNA-FISH**

856 Livers were fixed in 4% paraformaldehyde (PFA) for 3 hours, cryoprotected in PFA + 30
857 % sucrose for overnight, embedded in OCT, and tissue blocks were kept at -80 °C until
858 sectioning. After sectioned at 8-10 μm thickness, the sections were post-fixed,
859 permeabilized with ethanol, and treated with proteinase K prior to hybridization as
860 previously described[5]. HCR RNA-FISH probes (Molecular Instruments) targeting *Pck1*
861 (B3), *Fasn* (B1), and *Glul* (B2) were hybridized overnight at 37 °C (0.4 pmol of each
862 probe set/100 uL). Once excess probes were removed, the amplification stage was
863 performed according to the manufacture's protocol for 12 hours (B3=546, B1=647,
864 B2=488, 6 pmol each of hairpin/100 uL)[39]. Sections were then washed, counterstained
865 with DAPI, and mounted with antifade medium. Images were acquired on an upright,
866 wide-field Olympus BX- 63 Microscope equipped with a Super Apochromatic objective
867 lens (60×/1.35 N.A., Pixel size (x,y) = 107.5 nm, z-step = 300nm). MetaMorph software
868 (Molecular Devices, v7.10.1.161) was used for controlling microscope automation and
869 image acquisition. Pericentral hepatocytes were identified by *Glul* expression, and
870 periportal hepatocytes were identified by the bile duct-associated morphology. Liver
871 lobule images were taken by taking sequential images and processed on FIJI (v2.16.0).
872 Transcription site analysis in hepatic lobules was performed using SmallFish (v2.1.10),
873 a python implementation of FishQuant[40]. Cell segmentation was performed in 2D using
874 Cellpose (https://github.com/MouseLand/cellpose); and spot detection was performed
875 via big-fish package (https://github.com/fish-quant/big-fish).

876 **Stable isotope tracing analyses**

877 For pyruvate-to glucose tracing experiments, isolated hepatocytes ($1x10^5$ cells) were
878 incubated in KH buffer containing 1 mM [2,3-$^{13}C_2$] sodium pyruvate or unlabeled
879 pyruvate, 1 mM sodium lactate, 2 mM L-glutamine, and 1 mM BSA-conjugated palmitic
880 acid at 37 °C for 1 hour. 200 µL of the media was extracted with methanol containing 2-
881 deoxyglucose, centrifuged (13,100 × *g*, 10 min, 4 °C), and the supernatant was dried
882 under gentle nitrogen flow. Samples were then reacted with hydroxylanmine followed by
883 acetic anhydride as previously described[5]. After reconstitution in ethyl acetate, the
884 samples were analyzed by gas chromatography mass spectrometry (GC (7890)-MS
885 (5975C), Agilent) in chemical ionization (CI) mode using methane as the CI gas.
886 Mass isotopologue distributions were analyzed using MassHunter software (Agilent)
887 and corrected for natural isotope abundance. Glucose isotopologues are reported as
888 molar fractions (M0–M6). The sum of all isotopologues of the molecules, m_i (where i = 1
889 to 6), is equal to 1 or 100%. The labelled isotopologue fractions consist of a distribution
890 not affected by the dilution with unlabeled compounds, reported as $m_i/\Sigma m_i$, in percent.
891 The enrichment ΣM_n is the weighted sum of the labelled species ($\Sigma Mn = 1*M_1 + 2*M_2 +$
892 $3*M_3 + 4*M_4 + 5*M_5 + 6*M_6$) = average number of ^{13}C carbons/molecule as previously
893 reported[5].

894 For *in vivo* deuterium labeling, mice were subjected to time-restricted feeding as
895 described above. For fed conditions, mice received an intraperitoneal (IP) injection of
896 0.9% NaCl in deuterated water (30 µL/g body weight) at 07:00, after which drinking
897 water was replaced with 6% ^2H_2O. Chow and 6 % ^2H_2O with 20 % sucrose (w/v) were
898 provided at 09:00, and mice were sacrificed at 13:00. For fasted conditions, mice were

899 fed chow and sucrose water (without $^{2}H_2O$) from 09:00 to 13:00, fasted for 24 h, injected
900 with $^{2}H_2O$ and regular drinking water was replaced with 6 % $^{2}H_2O$ water at 07:00 the
901 following day, and sacrificed at 13:00. Lipids were extracted from isolated hepatocytes
902 ($1x10^6$ cells) following alkaline saponification in 1 M NaOH in 70 % ethanol in water with
903 heptadecanoic acid (C17:0) as an internal standard. Extracted fatty acids were
904 derivatized with BSTFA and analyzed by GC-MS (Agilent) with a DB-5MS column.
905 Palmitate deuterium enrichment was quantified from the m/z 313 fragment and
906 calculated. The total labeled fraction of palmitate was calculated with fraction
907 enrichment. The total palmitate was calculated relative to the concentration of
908 heptadecanoic acid. The newly synthesized palmitate was calculated with the function:
909 Newly synthesized palmitate = Total palmitate * total fraction of labeled
910 palmitate/deuterium enrichment in plasma/tissue weight.

911 **^{18}O water labeling in vivo**

912 Mice were subjected to time-restricted feeding as described above. In both fed and
913 fasted conditions, the mice were gavage with ^{18}O water or regular water at 12:48,
914 received IP injection of ^{18}O water or regular water at 12:53, then sacrificed at 13:00. The
915 liver was rinsed with 150 mM ammonium acetate before frozen in pre-chilled
916 isopentane. A 20 um thickness of tissue section was used for DESI imaging. The slide
917 was analyzed with a Waters Cyclic Ion Mobility-Mass Spectrometry (Cyclic-iMS).
918 The slide was placed in desiccator for about half an hour before loading into DESI
919 stage. The solvent was methanol:water=60:40(v:v) with 200ng/mL LeuEnk. The flow
920 rate was set to 2 μL/min. The resolution was set to 60um with 300 μm/sec. The mass

921 range was set to 50 – 1200 m/z, and the mobility was set to 1 pass with TW ramp of
922 TOF settings are 16 – 28 V/ms.

923 **DESI and MALDI metabolic spatial imaging**

924 Mice were subjected to time-restricted feeding as described above. On the day of the
925 experiment, mice were provided with D17011901px (Modified OSD with Macronutrient
926 Content Similar to LabDiet 5053) with $^{13}C_6$ glucose or unlabeled glucose (for 1 g of
927 premix, 1.31 g of glucose was added) at 9:00. Mice were then sacrificed at 13:00,
928 corresponding to 4 hours of feeding, and the liver was frozen in pre-chilled isopentane.
929 For DESI analysis, the slices were sectioned into 20um thickness. The ^{13}C samples was
930 analyzed with DESI-Xevo TQ absolute MS (Waters). The solvent was
931 methanol:water=80:20(v:v) with 200ng/mL LeuEnk with a flow rate of 1.2ul/mL and was
932 scanned with 25 x 25 um spatial resolution. The metabolites and their isotopolgues was
933 analyzed in the negative multiple reaction monitoring (MRM) mode. The data was
934 processed with HDI software (Waters).

935 **PrimeFlow**

936 After isolating hepatocytes as described above, the hepatocytes went through the
937 PrimeFlow (Invitrogen, #88-18005-204) protocol based on the manufacturer's
938 instructions with minor modifications. Briefly, hepatocytes were fixed using PrimeFlow
939 RNA Fixation Buffers. Cells were then permeabilized in PrimeFlow RNA
940 Permeabilization Buffer supplemented with RNase inhibitors, followed by a second
941 fixation step. After washing, cells were hybridized with target-specific RNA probe sets
942 diluted in PrimeFlow RNA Target Probe Diluent for 2 hours at 40 °C. Samples were
943 washed in PrimeFlow RNA Wash Buffer containing RNase inhibitor and stored

944 overnight at 2-8 °C in the dark. On the following day, signal amplification was performed
945 through sequential incubations with PreAmp Mix, Amp Mix, and fluorescently labeled
946 probes, each at 40 °C, with intervening washes according to the manufacturer's
947 instructions. Following the final labeling step, cells were washed, resuspended in
948 PrimeFlow RNA Storage Buffer and analyzed on BD FACSAria III. All centrifugation
949 steps were done at 800 × *g* unless otherwise specified.

950 **Hyperinsulinemic-euglycemic clamp experiments**

951 Hyperinsulinemic-euglycemic clamp studies were performed in conscious, unrestrained
952 mice. Briefly, mice were surgically implanted with catheters in the jugular vein for
953 infusions and the carotid artery for blood sampling. After recovering for at least 3 days
954 following surgery, the mice were subjected to time-restricted feeding as described
955 above. On the day of the experiment, catheters were connected to infusion lines, and
956 basal blood glucose was measured from the arterial blood using a glucometer.
957 Continuous insulin was infused at the indicated rates and maintained for 2 hours. Blood
958 glucose was clamped at 150 mg/dL by a variable infusion of 20% glucose solution,
959 adjusted based on blood glucose measurements every 10-20 minutes. At the end of the
960 clamp, liver perfusion for total hepatocyte isolation was performed.

961 **Spatial Transcriptomics**

962 For high-fat diet studies, fresh frozen mouse livers were embedded in Neg-50 and
963 stored at -80 °C until sectioning. After sectioned at 10 μm thickness, **s**ections were
964 adhered to capture areas by brief warming onto Visium v1 slides (10x Genomics). For
965 humanized liver studies, livers were fixed in 4% paraformaldehyde (PFA) for 3 hours,
966 cryoprotected in PFA + 30 % sucrose for overnight, embedded in OCT, and tissue

967 blocks were kept at -80 °C until sectioning. After sectioned at 10 μm thickness, Visium
968 v2 (prepared with CytAssist) was performed using the CytAssist instrument. For both
969 studies, the sample preparation was performed according to the manufacturer's
970 guidelines. Briefly, tissue sections were stained with hematoxylin and eosin (H&E),
971 imaged using a brightfield microscope for histological reference and spatial registration.
972 RNA capture, reverse transcription, second-strand synthesis, cDNA amplification, and
973 library construction were performed. Libraries were indexed, quality-controlled, and
974 sequenced on an Illumina platform using paired-end sequencing. Raw sequencing data
975 were processed using Space Ranger (v2.0.0 for high-fat diet studies with reference
976 genome: mm10-2020-A, v3.1.0 for humanized liver studies with reference genome:
977 GRCh38-2020-A, 10x Genomics) to align reads to the reference genome and generate
978 spatial gene expression matrices. Spatial alignment was performed using H&E images,
979 and downstream analyses were conducted using standard single-cell and spatial
980 transcriptomics workflows.

981 **QUANTIFICATION AND STATISTICAL ANALYSIS**

982 Excel (v16.101.3), Prism (v10.6.1) GraphPad Software, were used for data processing,
983 analyses, and graph productions in the experiments. All data are presented as the
984 mean +/- standard deviation unless otherwise noted. Student's *t*-test with unpaired two-
985 tailed p values of *$p<0.05$, **$p<0.01$, and ***$p<0.001$ was considered statistically
986 significant when comparing two groups. (N.S.=not statistically significant).
987 Figures/Images were created by Powerpoint (v16.101.3), IGV (v2.19.7), Loupe Browser
988 (v9.0.0), FIJI (v2.16.0), QuPath (v0.6.0) and Adobe Illustrator (v28.1).
989

990 **REFERENCES**

991 1 Ben-Moshe, S. & Itzkovitz, S. Spatial heterogeneity in the mammalian liver. *Nat*
992 *Rev Gastroenterol Hepatol* **16**, 395-410 (2019). https://doi.org:10.1038/s41575-
993 019-0134-x
994 2 Martini, T., Naef, F. & Tchorz, J. S. Spatiotemporal Metabolic Liver Zonation and
995 Consequences on Pathophysiology. *Annu Rev Pathol* **18**, 439-466 (2023).
996 https://doi.org:10.1146/annurev-pathmechdis-031521-024831
997 3 Halpern, K. B. *et al.* Single-cell spatial reconstruction reveals global division of
998 labour in the mammalian liver. *Nature* **542**, 352-356 (2017).
999 https://doi.org:10.1038/nature21065
1000 4 Rosenberger, F. A. *et al.* Spatial single-cell mass spectrometry defines zonation
1001 of the hepatocyte proteome. *Nat Methods* **20**, 1530-1536 (2023).
1002 https://doi.org:10.1038/s41592-023-02007-6
1003 5 Okada, J. *et al.* Spatial hepatocyte plasticity of gluconeogenesis during the
1004 metabolic transitions between fed, fasted and starvation states. *Nat Metab* **7**,
1005 1073-1091 (2025). https://doi.org:10.1038/s42255-025-01269-y
1006 6 Sasse, D., Katz, N. & Jungermann, K. Functional heterogeneity of rat liver
1007 parenchyma and of isolated hepatocytes. *FEBS Lett* **57**, 83-88 (1975).
1008 https://doi.org:10.1016/0014-5793(75)80157-8
1009 7 Wagle, S. R., Ingebretsen, W. R. & Sampson, L. Studies on gluconeogenesis
1010 and stimulation of glycogen and protein synthesis in isolated hepatocytes in
1011 alloxan diabetic, normal fed and fasted animals. *Acta Diabetol Lat* **12**, 185-198
1012 (1975). https://doi.org:10.1007/BF02581299
1013 8 Bartels, H., Vogt, B. & Jungermann, K. Glycogen synthesis via the indirect
1014 gluconeogenic pathway in the periportal and via the direct glucose utilizing
1015 pathway in the perivenous zone of perfused rat liver. *Histochemistry* **89**, 253-260
1016 (1988). https://doi.org:10.1007/BF00493149
1017 9 Petersen, M. C., Vatner, D. F. & Shulman, G. I. Regulation of hepatic glucose
1018 metabolism in health and disease. *Nat Rev Endocrinol* **13**, 572-587 (2017).
1019 https://doi.org:10.1038/nrendo.2017.80
1020 10 Coelho, M. *et al.* Enrichment of hepatic glycogen and plasma glucose from
1021 H(2)(18) O informs gluconeogenic and indirect pathway fluxes in naturally
1022 feeding mice. *NMR Biomed* **36**, e4837 (2023). https://doi.org:10.1002/nbm.4837
1023 11 Adeva-Andany, M. M., Gonzalez-Lucan, M., Donapetry-Garcia, C., Fernandez-
1024 Fernandez, C. & Ameneiros-Rodriguez, E. Glycogen metabolism in humans.
1025 *BBA Clin* **5**, 85-100 (2016). https://doi.org:10.1016/j.bbacli.2016.02.001
1026 12 Youn, D. Y. *et al.* The Mediator complex kinase module is necessary for fructose
1027 regulation of liver glycogen levels through induction of glucose-6-phosphatase
1028 catalytic subunit (G6pc). *Mol Metab* **48**, 101227 (2021).
1029 https://doi.org:10.1016/j.molmet.2021.101227
1030 13 Core, L. & Adelman, K. Promoter-proximal pausing of RNA polymerase II: a
1031 nexus of gene regulation. *Genes Dev* **33**, 960-982 (2019).
1032 https://doi.org:10.1101/gad.325142.119

1033 14 Chen, K. S. & Katz, J. Zonation of glycogen and glucose syntheses, but not
1034 glycolysis, in rat liver. *Biochem J* **255**, 99-104 (1988).
1035 https://doi.org:10.1042/bj2550099
1036 15 Quistorff, B. Gluconeogenesis in periportal and perivenous hepatocytes of rat
1037 liver, isolated by a new high-yield digitonin/collagenase perfusion technique.
1038 *Biochem J* **229**, 221-226 (1985). https://doi.org:10.1042/bj2290221
1039 16 Droin, C. *et al.* Space-time logic of liver gene expression at sub-lobular scale. *Nat*
1040 *Metab* **3**, 43-58 (2021). https://doi.org:10.1038/s42255-020-00323-1
1041 17 Henning, A. L., Sampson, J. N. B. & McFarlin, B. K. Measurement of Low-
1042 Abundance Intracellular mRNA Using Amplified FISH Staining and Image-Based
1043 Flow Cytometry. *Curr Protoc Cytom* **76**, 7 46 41-47 46 48 (2016).
1044 https://doi.org:10.1002/0471142956.cy0746s76
1045 18 Zeleznikar, R. J. & Goldberg, N. D. Kinetics and compartmentation of energy
1046 metabolism in intact skeletal muscle determined from 18O labeling of metabolite
1047 phosphoryls. *J Biol Chem* **266**, 15110-15119 (1991).
1048 19 Goldberg, N. D., Ames, A. A., 3rd, Gander, J. E. & Walseth, T. F. Magnitude of
1049 increase in retinal cGMP metabolic flux determined by 18O incorporation into
1050 nucleotide alpha-phosphoryls corresponds with intensity of photic stimulation. *J*
1051 *Biol Chem* **258**, 9213-9219 (1983).
1052 20 Walseth, T. F., Gander, J. E., Eide, S. J., Krick, T. P. & Goldberg, N. D. 18O
1053 labeling of adenine nucleotide alpha-phosphoryls in platelets. Contribution by
1054 phosphodiesterase-catalyzed hydrolysis of cAMP. *J Biol Chem* **258**, 1544-1558
1055 (1983).
1056 21 Dawis, S. M. *et al.* Adenosine triphosphate utilization rates and metabolic pool
1057 sizes in intact cells measured by transfer of 18O from water. *Biophys J* **55**, 79-99
1058 (1989). https://doi.org:10.1016/S0006-3495(89)82782-1
1059 22 Zeleznikar, R. J. *et al.* Evidence for compartmentalized adenylate kinase
1060 catalysis serving a high energy phosphoryl transfer function in rat skeletal
1061 muscle. *J Biol Chem* **265**, 300-311 (1990).
1062 23 Tang, Y. *et al.* TIGAR deficiency enhances skeletal muscle thermogenesis by
1063 increasing neuromuscular junction cholinergic signaling. *Elife* **11** (2022).
1064 https://doi.org:10.7554/eLife.73360
1065 24 Hall, A. *et al.* Transaminase abnormalities and adaptations of the liver lobule
1066 manifest at specific cut-offs of steatosis. *Sci Rep* **7**, 40977 (2017).
1067 https://doi.org:10.1038/srep40977
1068 25 Sugahara, G., Ishida, Y., Sun, J., Tateno, C. & Saito, T. Art of Making Artificial
1069 Liver: Depicting Human Liver Biology and Diseases in Mice. *Semin Liver Dis* **40**,
1070 189-212 (2020). https://doi.org:10.1055/s-0040-1701444
1071 26 Seubnooch, P. *et al.* Characterisation of hepatic lipid signature distributed across
1072 the liver zonation using mass spectrometry imaging. *JHEP Rep* **5**, 100725
1073 (2023). https://doi.org:10.1016/j.jhepr.2023.100725
1074 27 Hatting, M., Tavares, C. D. J., Sharabi, K., Rines, A. K. & Puigserver, P. Insulin
1075 regulation of gluconeogenesis. *Ann N Y Acad Sci* **1411**, 21-35 (2018).
1076 https://doi.org:10.1111/nyas.13435

1077 28 Sahoo, B., Srivastava, M., Katiyar, A., Ecelbarger, C. & Tiwari, S. Liver or kidney:
1078 Who has the oar in the gluconeogenesis boat and when? *World J Diabetes* **14**,
1079 1049-1056 (2023). https://doi.org:10.4239/wjd.v14.i7.1049
1080 29 Mutel, E. *et al.* Control of blood glucose in the absence of hepatic glucose
1081 production during prolonged fasting in mice: induction of renal and intestinal
1082 gluconeogenesis by glucagon. *Diabetes* **60**, 3121-3131 (2011).
1083 https://doi.org:10.2337/db11-0571
1084 30 Edgerton, D. S. *et al.* Insulin's direct hepatic effect explains the inhibition of
1085 glucose production caused by insulin secretion. *JCI Insight* **2**, e91863 (2017).
1086 https://doi.org:10.1172/jci.insight.91863
1087 31 Buettner, C. *et al.* Severe impairment in liver insulin signaling fails to alter hepatic
1088 insulin action in conscious mice. *J Clin Invest* **115**, 1306-1313 (2005).
1089 https://doi.org:10.1172/JCI23109
1090 32 Tosh, D., Alberti, G. M. & Agius, L. Glucagon regulation of gluconeogenesis and
1091 ketogenesis in periportal and perivenous rat hepatocytes. Heterogeneity of
1092 hormone action and of the mitochondrial redox state. *Biochem J* **256**, 197-204
1093 (1988). https://doi.org:10.1042/bj2560197
1094 33 Buglakova, E. *et al.* Spatial single-cell isotope tracing reveals heterogeneity of de
1095 novo fatty acid synthesis in cancer. *Nat Metab* **6**, 1695-1711 (2024).
1096 https://doi.org:10.1038/s42255-024-01118-4
1097 34 Langmead, B. & Salzberg, S. L. Fast gapped-read alignment with Bowtie 2. *Nat*
1098 *Methods* **9**, 357-359 (2012). https://doi.org:10.1038/nmeth.1923
1099 35 Li, H. A statistical framework for SNP calling, mutation discovery, association
1100 mapping and population genetical parameter estimation from sequencing data.
1101 *Bioinformatics* **27**, 2987-2993 (2011).
1102 https://doi.org:10.1093/bioinformatics/btr509
1103 36 Ramirez, F. *et al.* deepTools2: a next generation web server for deep-sequencing
1104 data analysis. *Nucleic Acids Res* **44**, W160-165 (2016).
1105 https://doi.org:10.1093/nar/gkw257
1106 37 Sullivan, A. E. & Santos, S. D. M. An Optimized Protocol for ChIP-Seq from
1107 Human Embryonic Stem Cell Cultures. *STAR Protoc* **1**, 100062 (2020).
1108 https://doi.org:10.1016/j.xpro.2020.100062
1109 38 Robinson, J. T. *et al.* Integrative genomics viewer. *Nat Biotechnol* **29**, 24-26
1110 (2011). https://doi.org:10.1038/nbt.1754
1111 39 Choi, H. M. *et al.* Programmable in situ amplification for multiplexed imaging of
1112 mRNA expression. *Nat Biotechnol* **28**, 1208-1212 (2010).
1113 https://doi.org:10.1038/nbt.1692
1114 40 Imbert, A. *et al.* FISH-quant v2: a scalable and modular tool for smFISH image
1115 analysis. *RNA* **28**, 786-795 (2022). https://doi.org:10.1261/rna.079073.121
1116

Figure 1 – *Pck1* is transcribed in hepatocytes the fed state

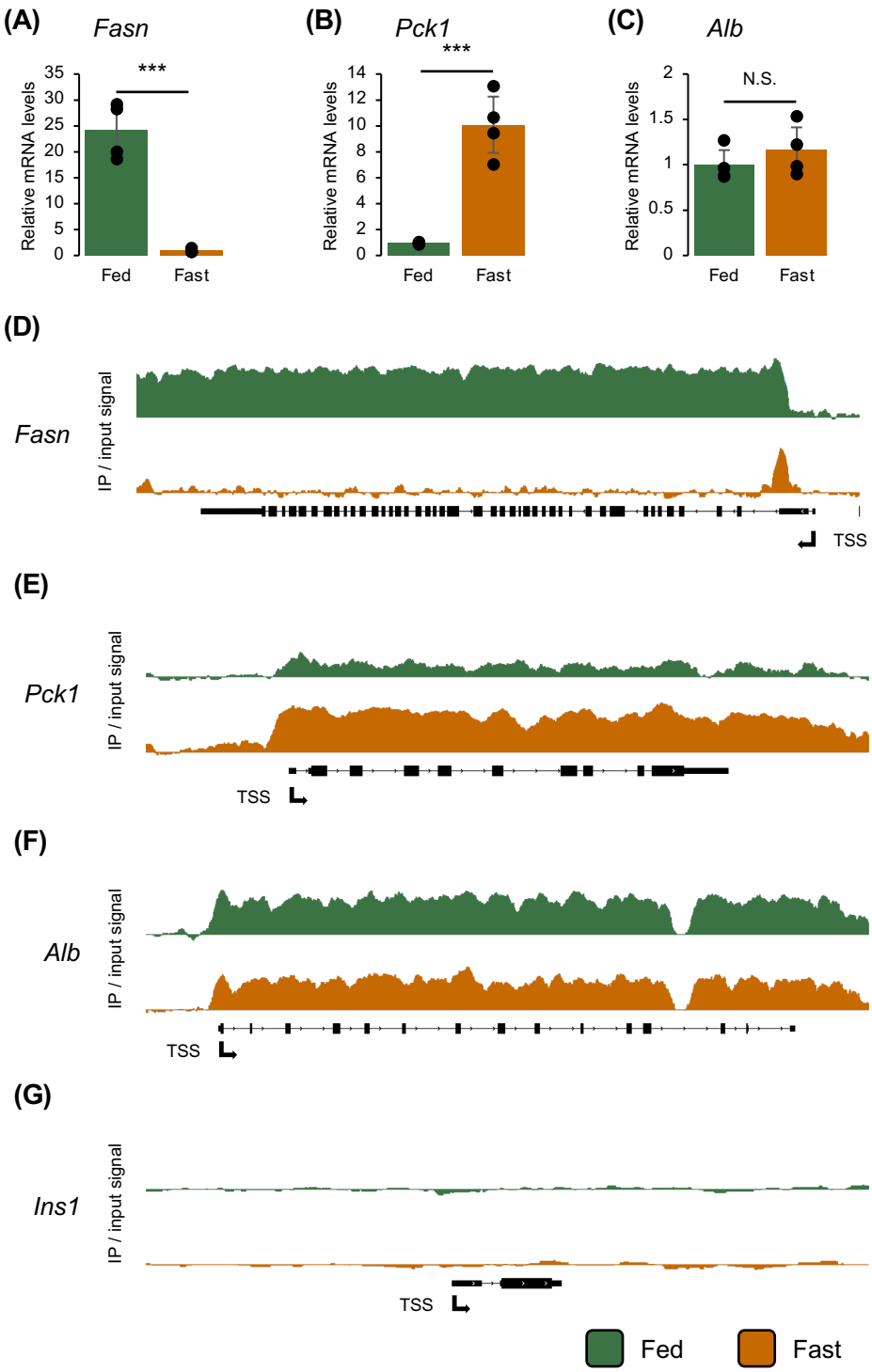

Figure 2 – *Fasn* and *Pck1* are co-expressed in a subset of periportal hepatocytes

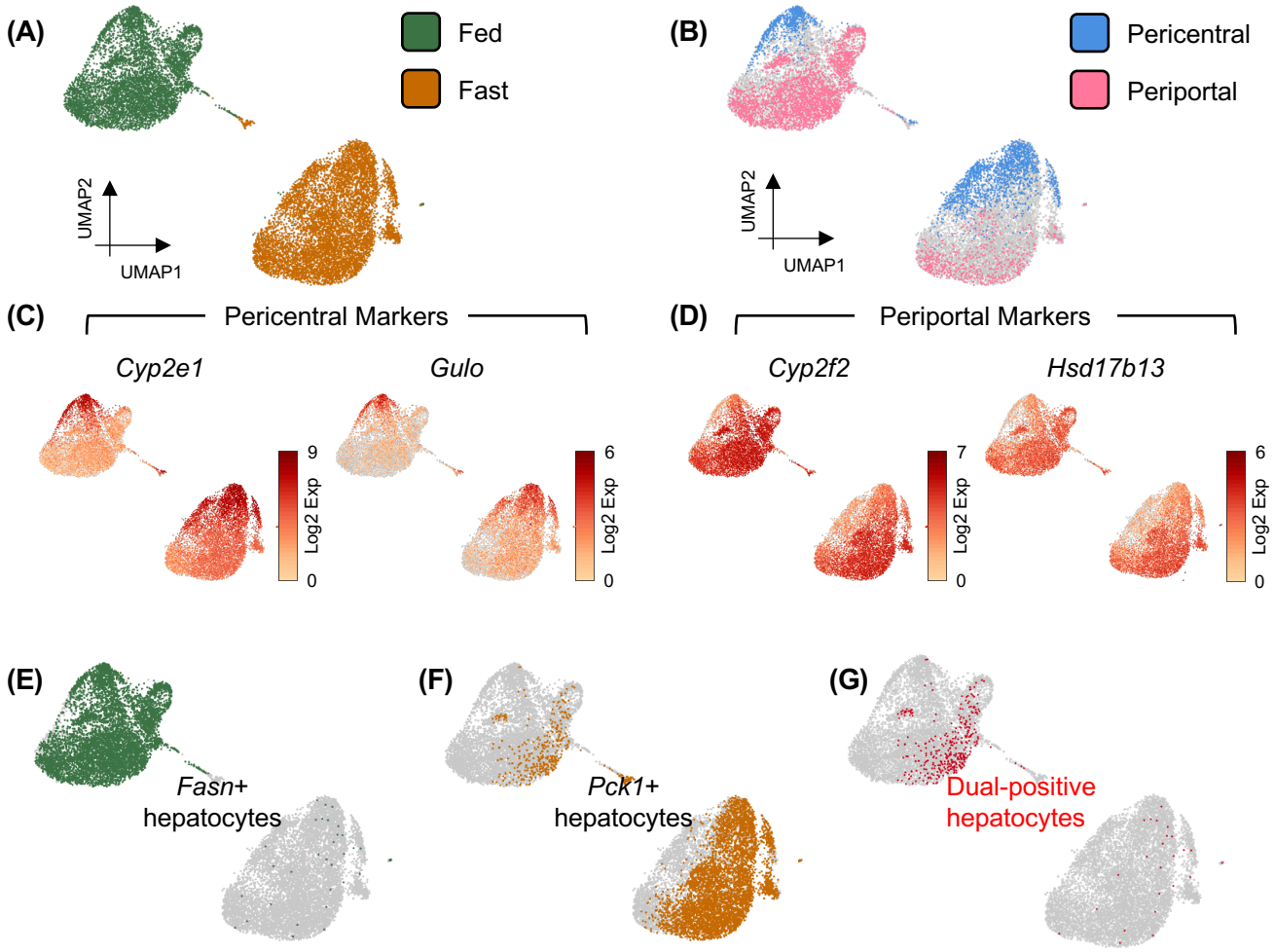

Figure 3 – *Fasn* and *Pck1* are actively co-transcribed in a subset of periportal hepatocytes

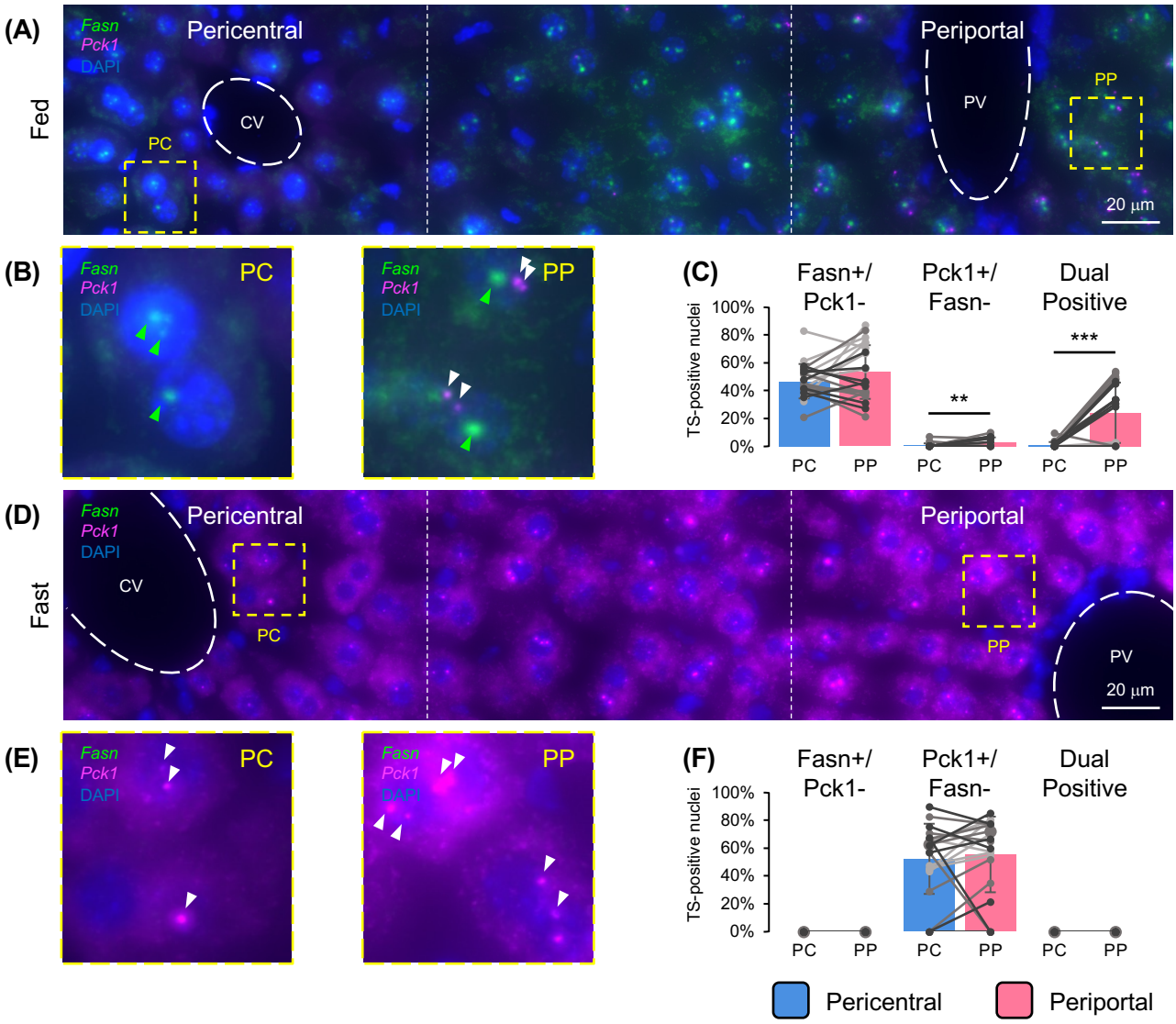

Figure 4 – Periportal hepatocytes have basal pyruvate-to-glucose flux in the fed state

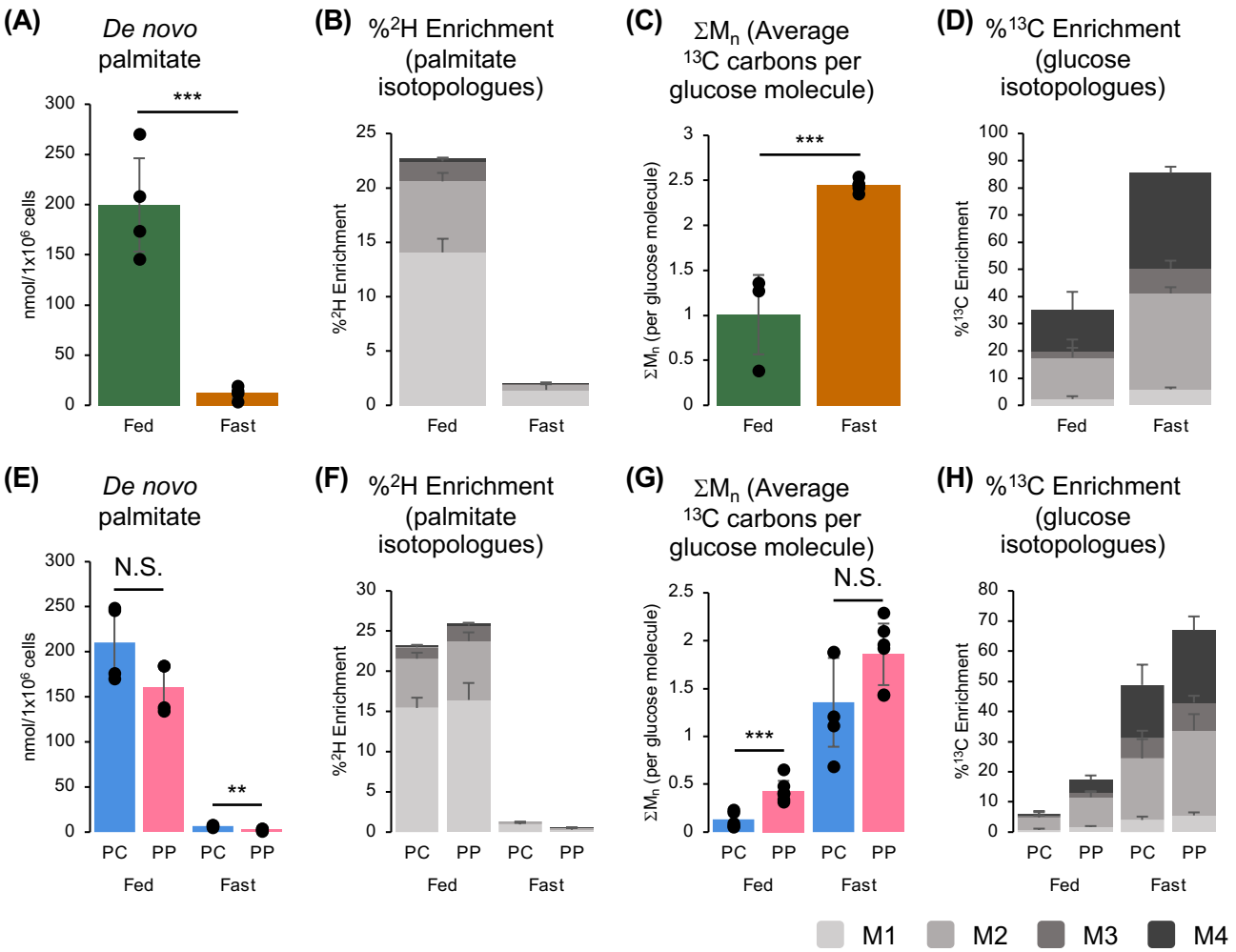

Figure 5 – A subset of liver regions has higher ATP turnover in the fed state

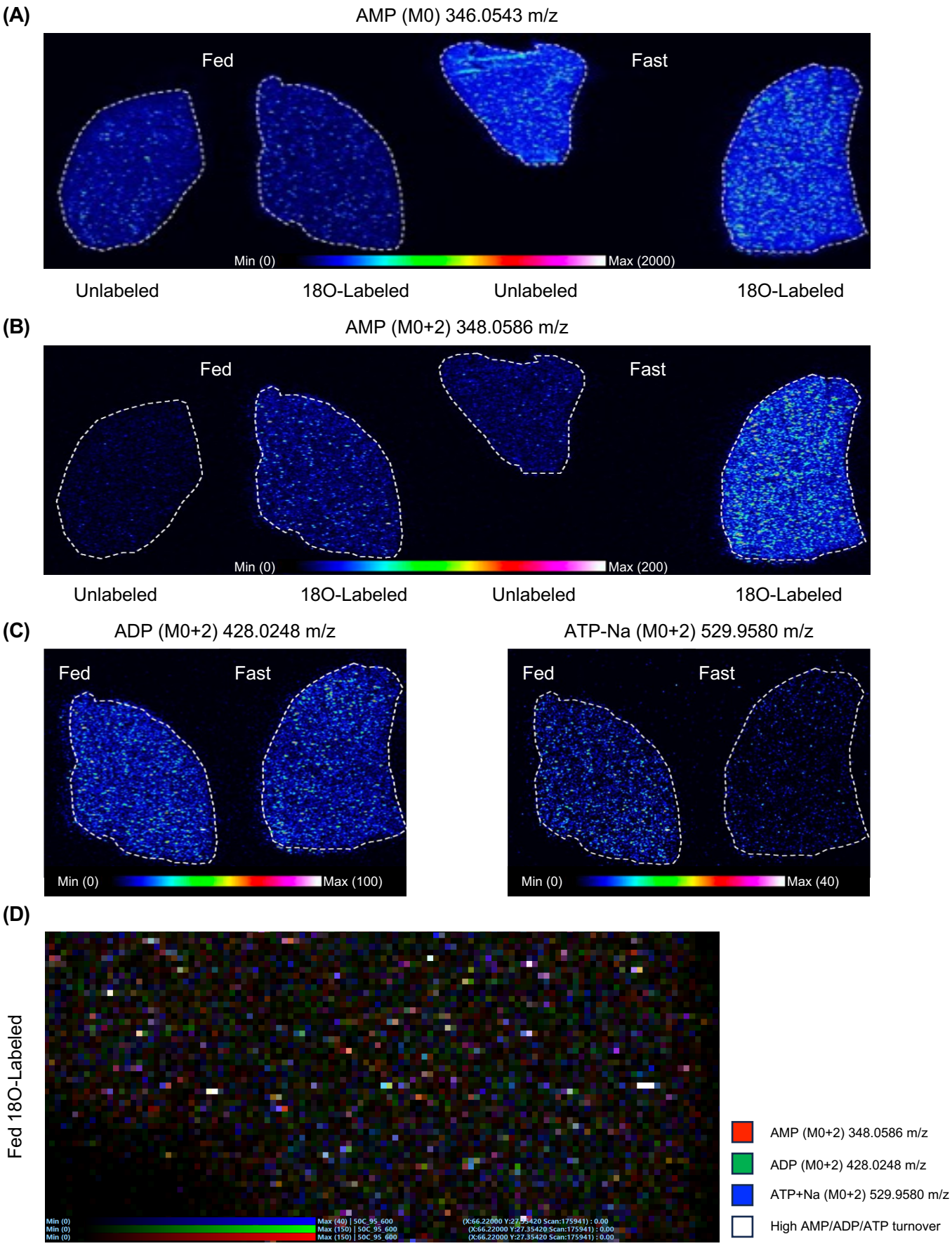

Figure 6 – A subset of hepatocytes is lipogenic and gluconeogenic

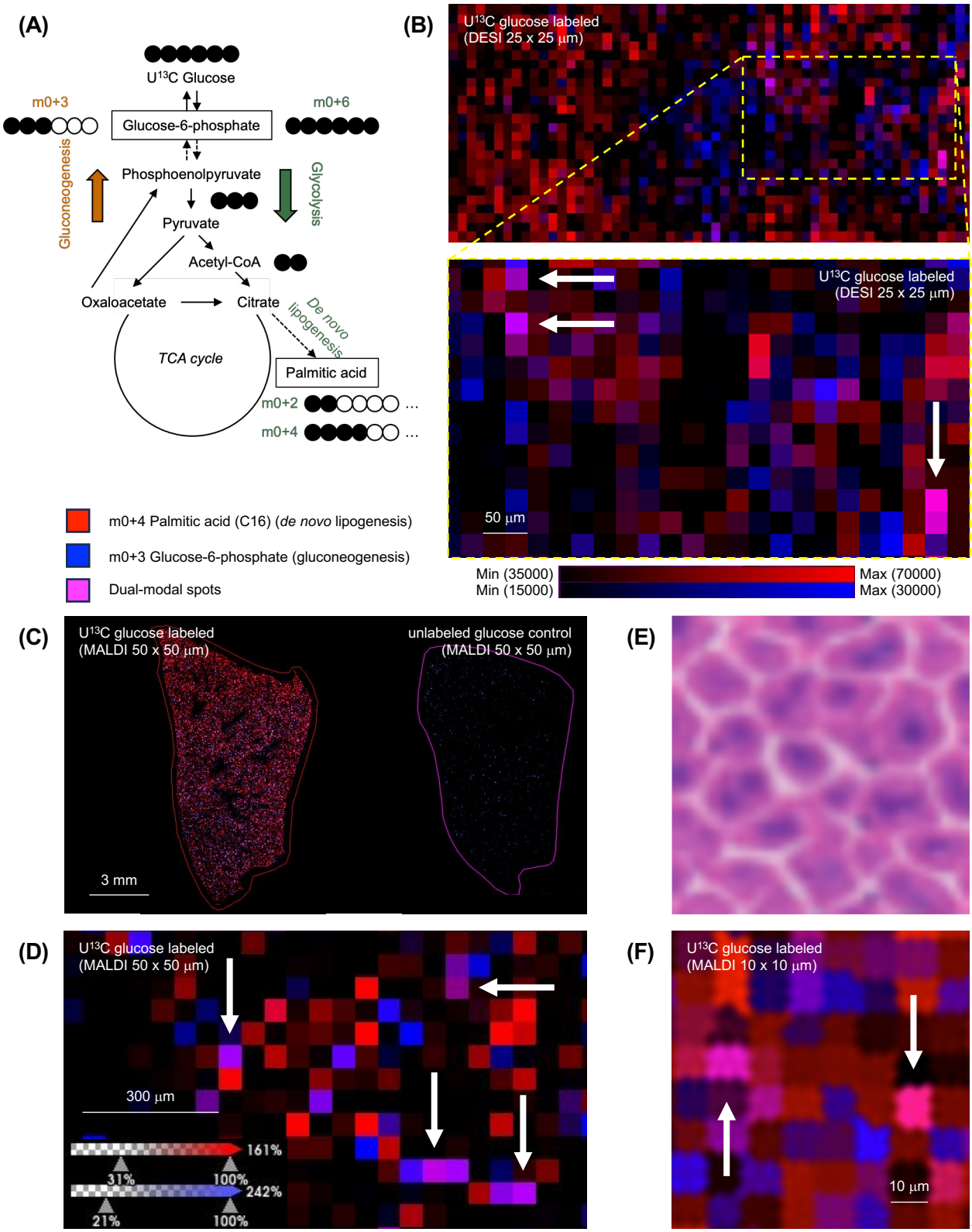

Figure 7 – Dual-positive spots increase in high-fat diet fed-mice liver

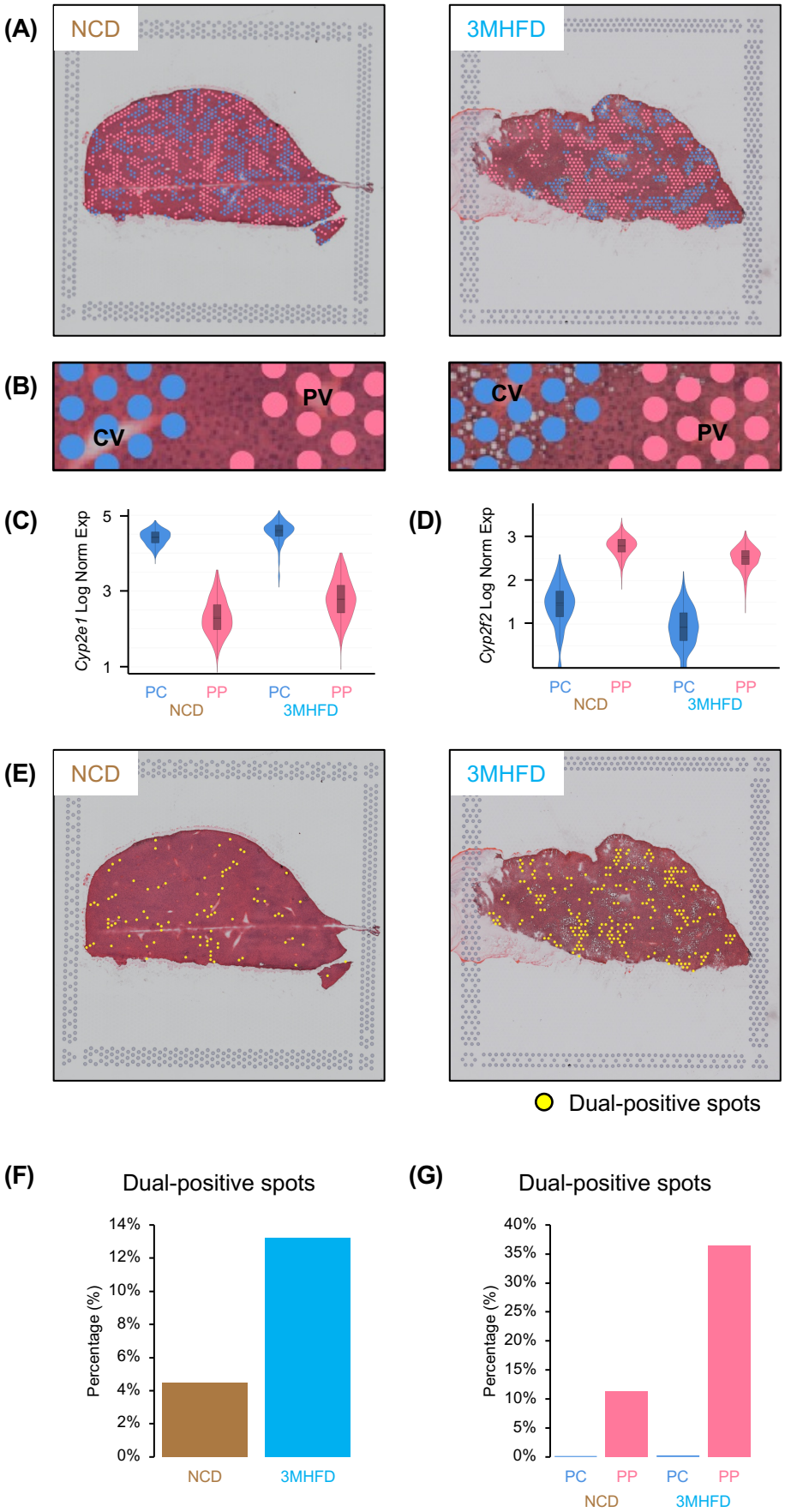

Supplementary Figures

Figure S1 – *G6pc* is transcribed in hepatocytes in the fed state

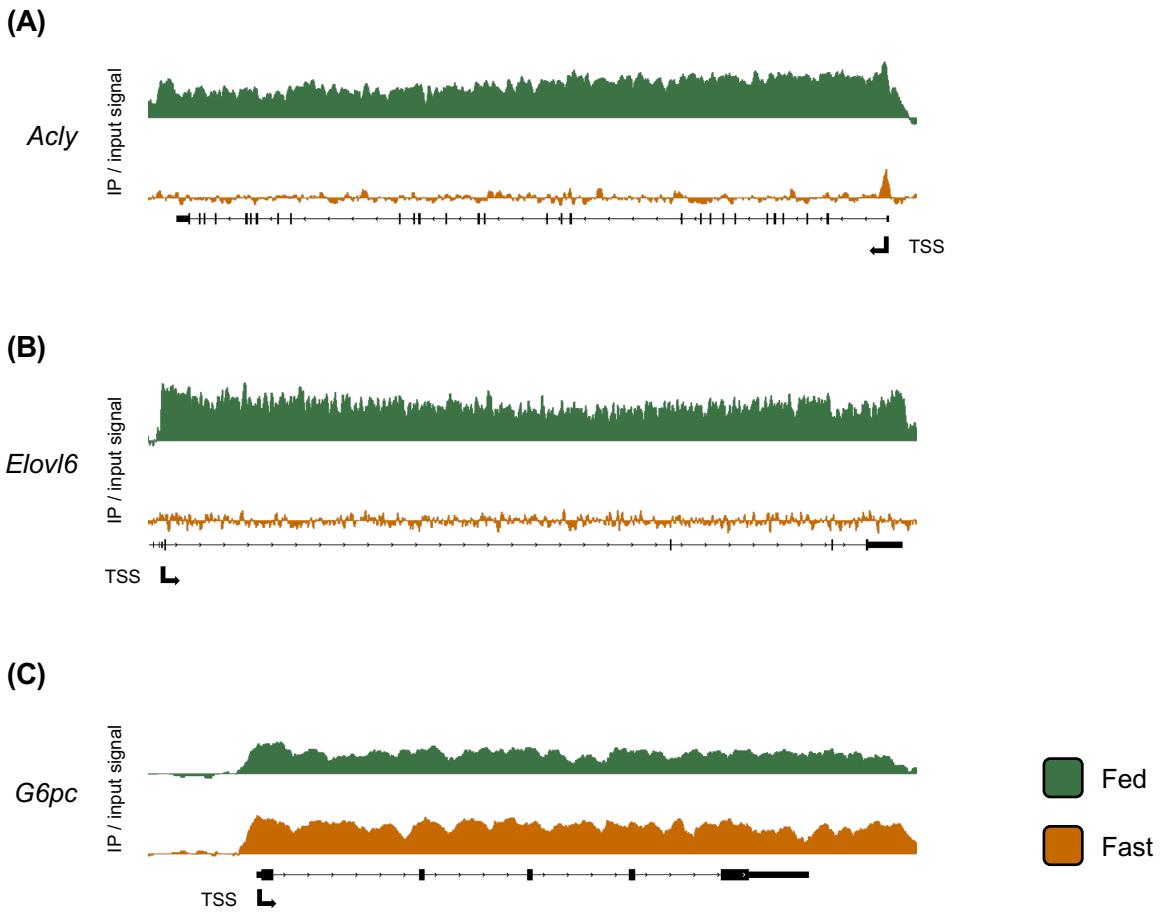

Figure S2 – *Pck1* is transcribed in periportal hepatocytes in the fed state

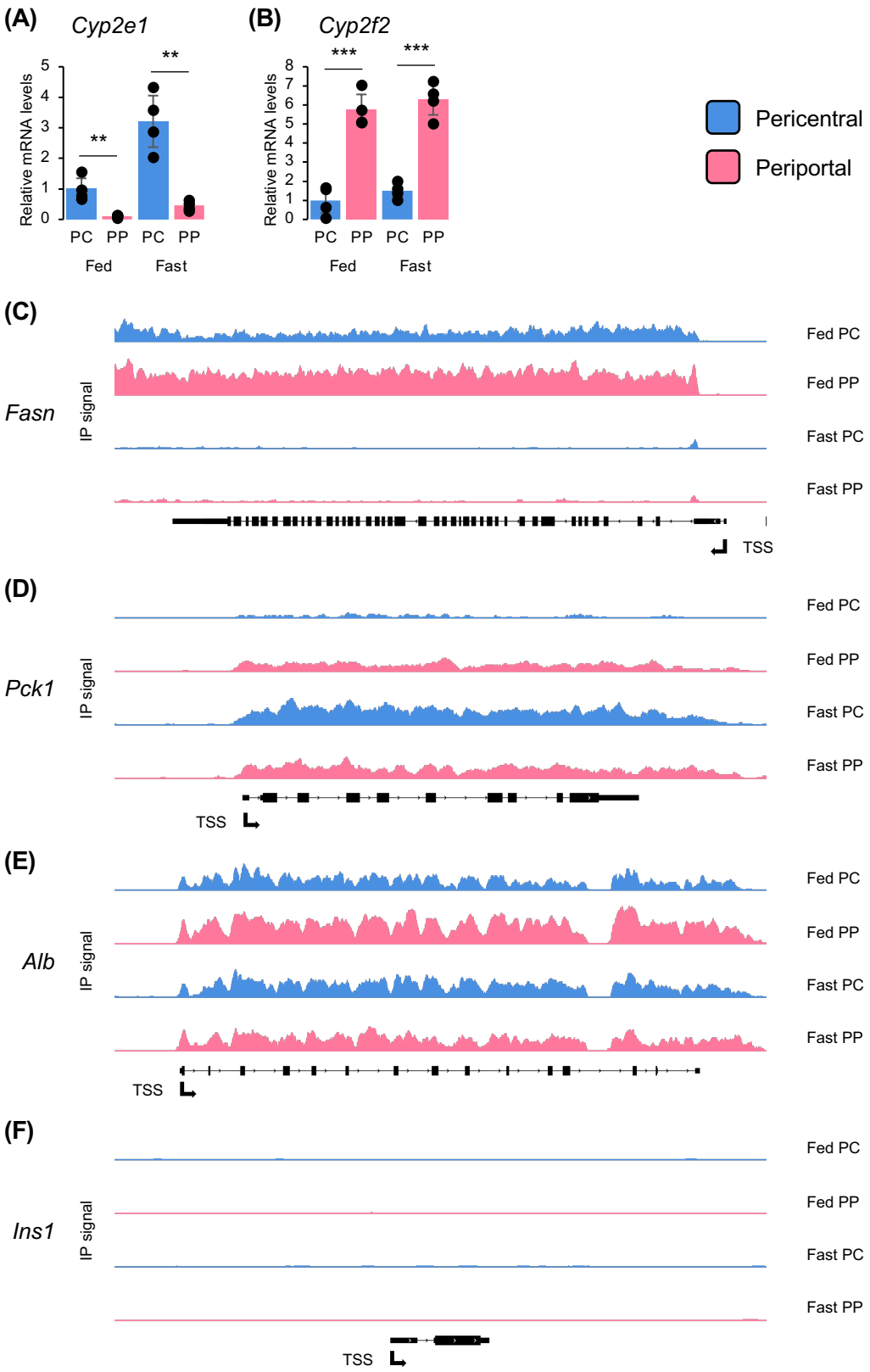

Figure S3 – Acly, Acaca, Elovl6, and G6pc are co-expressed in a subset of hepatocytes

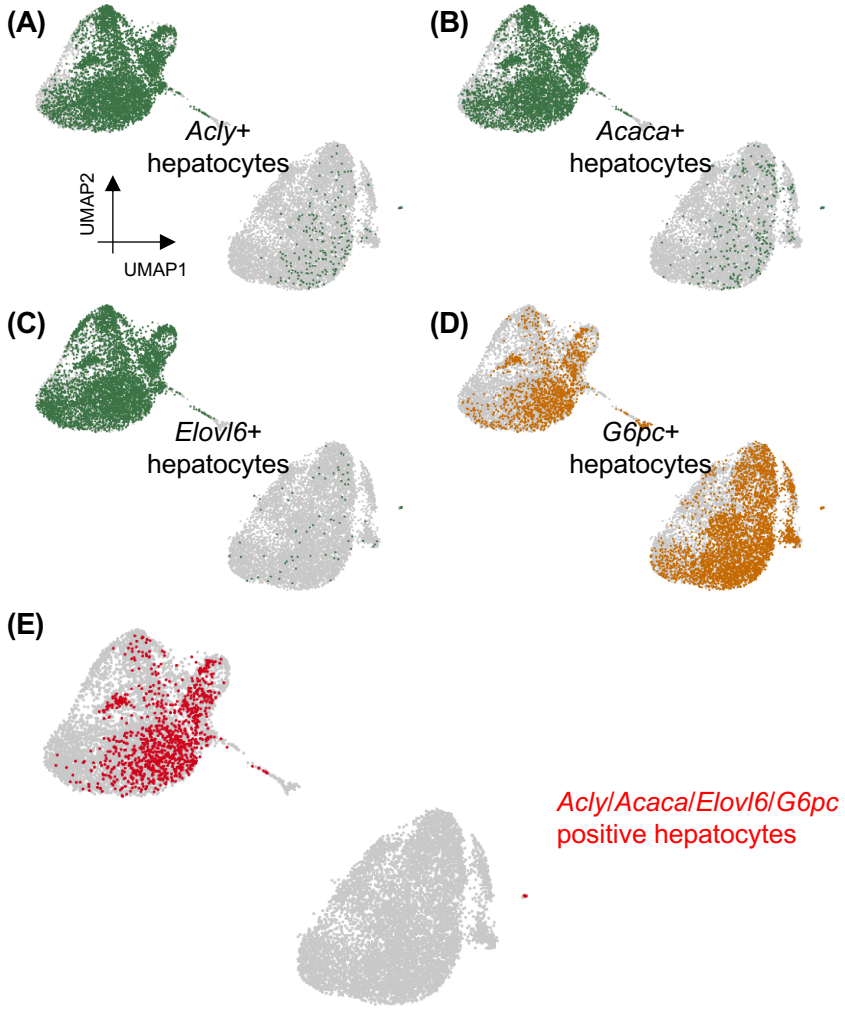

Figure S4 – *Pck1* is actively transcribed in the fed state

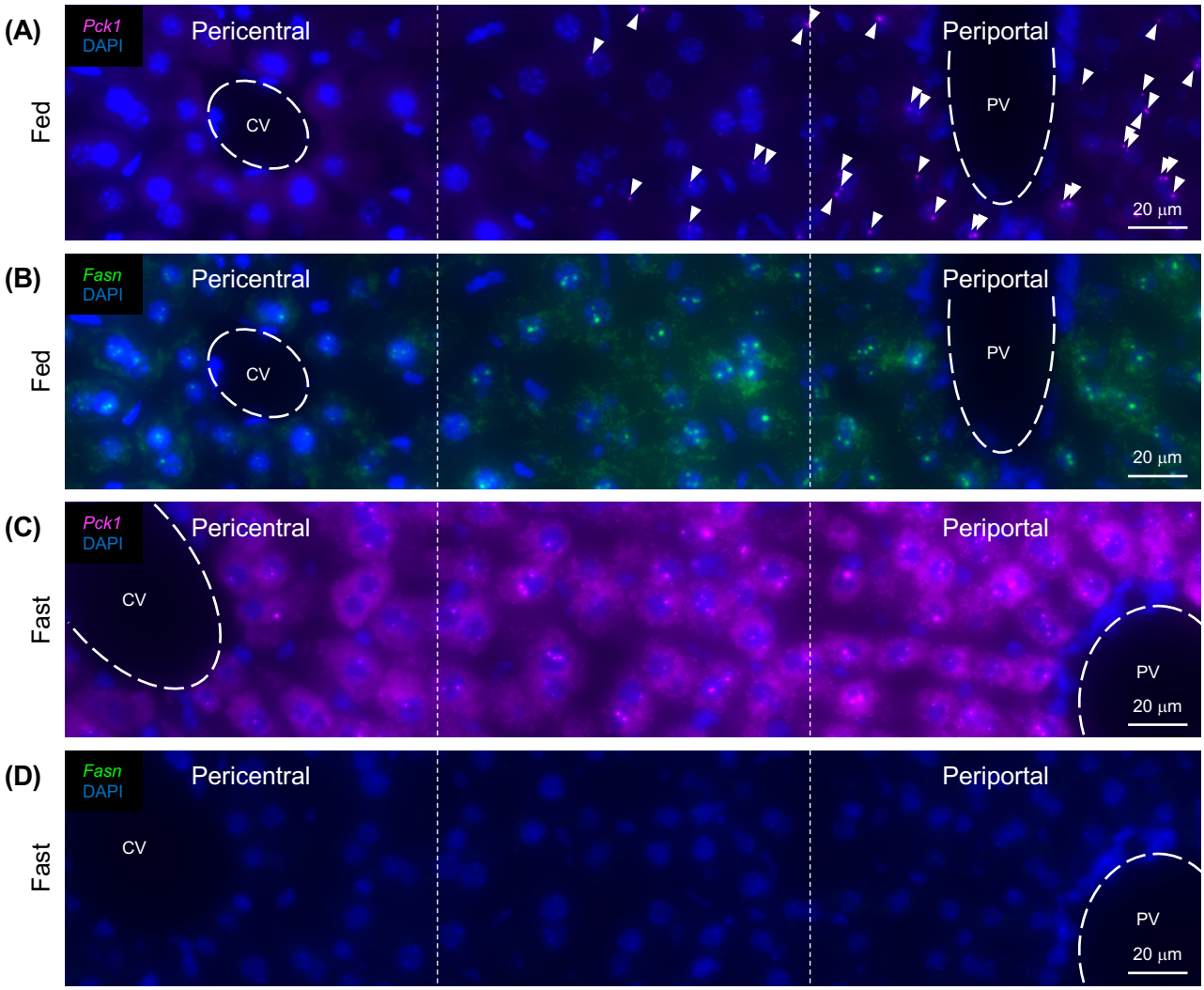

Figure S5 – Dual-positive hepatocytes are insulin resistant in suppression of *Pck1*

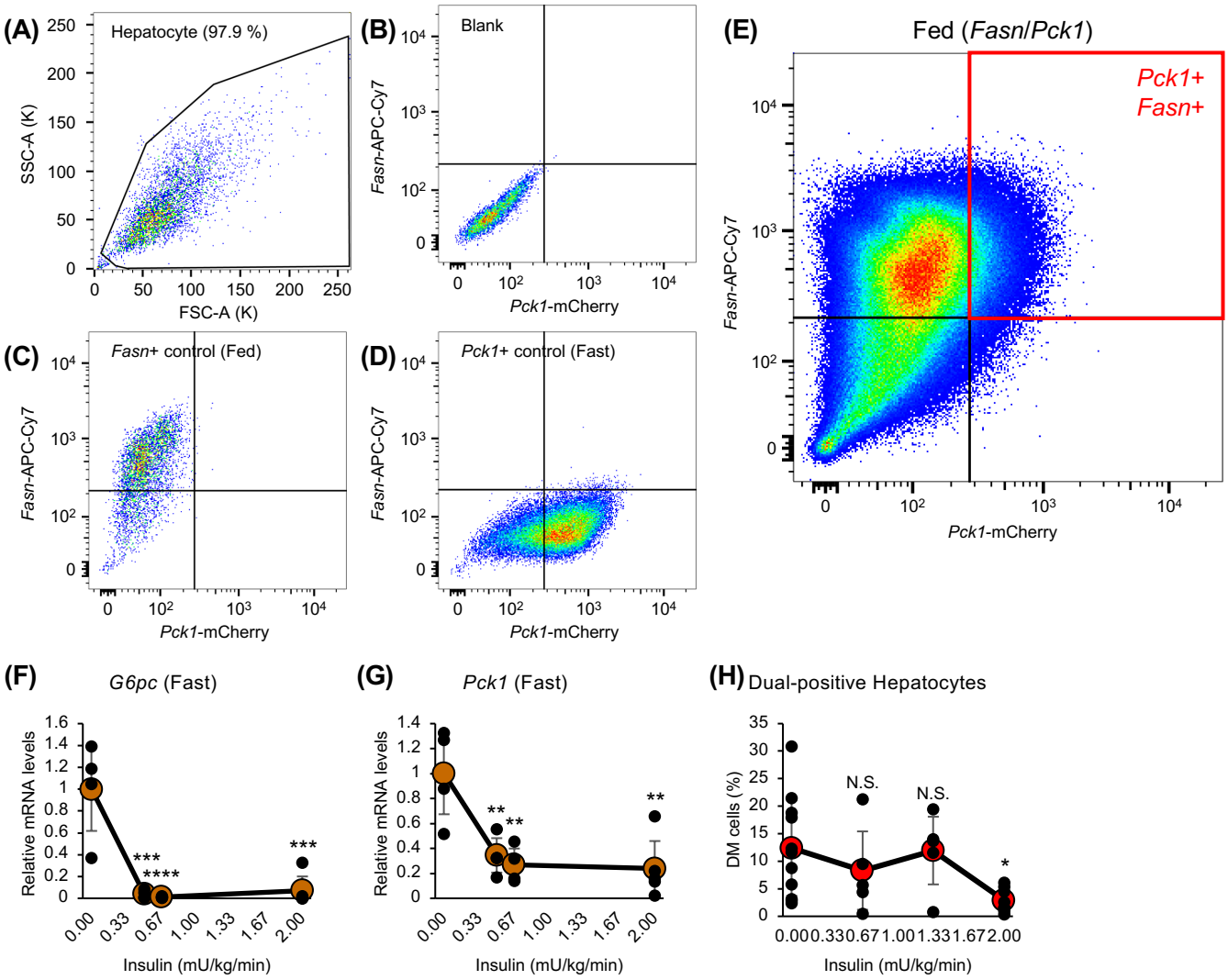

Figure S6 – Humanized mouse liver has dual-positive spots

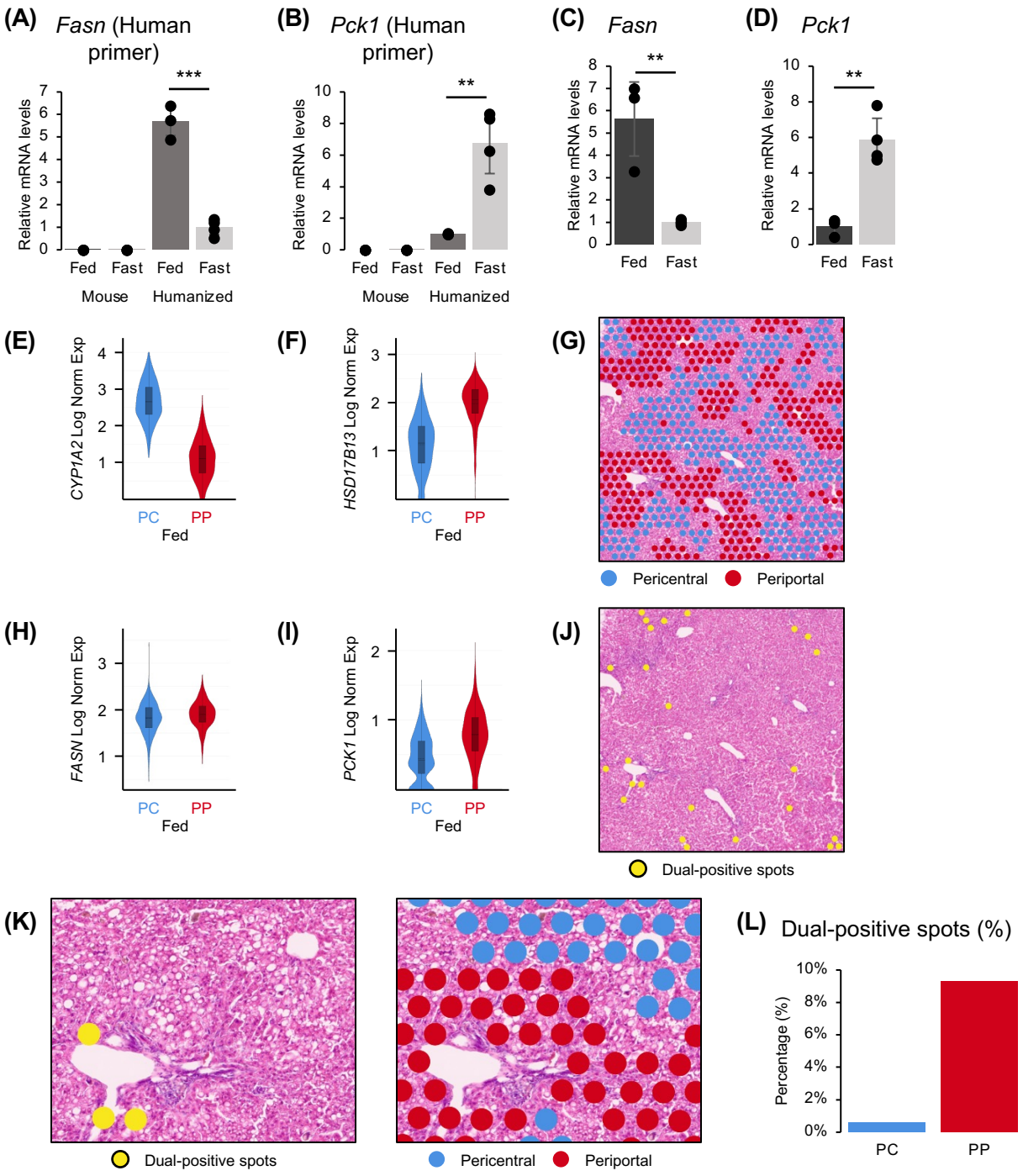

Figure S7 – t-SNE separates NCD and 3MHFD

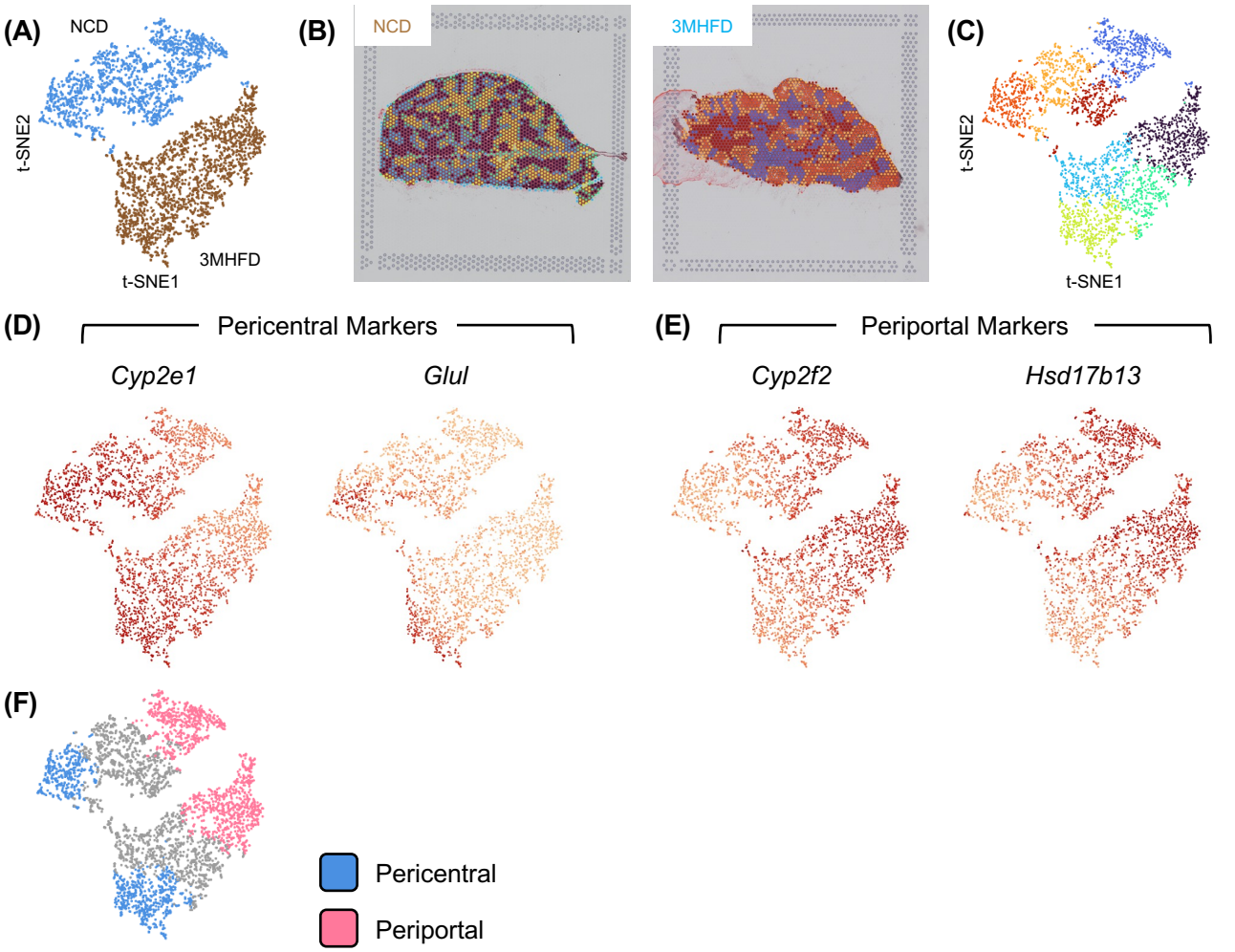

Table S1 – Compendium of $^{18}O/^{16}O$ exchange reactions which determine ATP turnover

Reaction:¤	Parameters:¤
γATP·+·[^{18}O]·H_2O·⟶·[^{18}O]·P_i·+·ADP¤	ATP·hydrolysis¤
[^{18}O]·P_i·+·ADP·⟶·[^{18}O]·γATP¤	ATP·synthesis¤
[^{18}O]·γATP·+·Cr·⟶·[^{18}O]·CrP·+·ADP¤	CK-catalyzed·phosphotransfer¤
[^{18}O]·γATP·+·AMP·⟶·[^{18}O]·βADP·+·ADP·⟶·[^{18}O]·βATP·+·AMP¤	AK-catalyzed·phosphotransfer¤

ATP turnover reflects the percentage of ^{16}O in ATP replaced by ^{18}O in the aliquot of cells analyzed, reflecting whole cell energetics. CK=creatine kinase, AK=adenylate kinase

Table S2 – Primer Sequences

Gene	Sequence (5' - 3')
Fasn _FWD (Mouse)	GGTCGTTTCTCCATTAAATTCTCAT
Fasn _REV (Mouse)	CTAGAAACTTTCCCAGAAATCTTCC
Pck1 _FWD (Mouse)	TCTCTGATCCAGACCTTCCAA
Pck1 _REV (Mouse)	GAAGTCCAGACCGTTATGCAG
Alb _FWD (Mouse)	CAAAGACGTGTGTTGCCGAT
Alb _REV (Mouse)	ACGGAGGTTTGGAATGGCAC
Cyp2e1 _FWD (Mouse)	CACAGCCAAGAACCCATGTACA
Cyp2e1 _REV (Mouse)	CAGGAGCCCATATCTCAGAGTTG
Cyp2f2 _FWD (Mouse)	CCTTTGACCCCGTGTTTATCC
Cyp2f2 _REV (Mouse)	TCGAAGCGACTTCCGAAGAC
Ppib _FWD (Mouse)	CAAGCATGTGGTTTTCGGCA
Ppib _REV (Mouse)	GCTGTCTGTCTTGGTGCTCT
Fasn _FWD (Human)	TTCTACGGCTCCACGCTCTTCC
Fasn _REV (Human)	GAAGAGTCTTCGTCAGCCAGGA
Pck1 _FWD (Human)	CATTGCCTGGATGAAGTTTGACG
Pck1 _REV (Human)	GGGTTGGTCTTCACTGAAGTCC
Ppib _FWD (Human)	AACGCAGGCAAAGACACCAACG
Ppib _REV (Human)	TCTGTCTTGGTGCTCTCCACCT